Pergamon

0301-9322(94)E0019-F

Int. J. Multiphase Flow Vol. 20, Suppl., pp. 233–259, 1994

0301-9322/94 $26.00 + 0.00

MASS FLUX, MASS FRACTION AND CONCENTRATION OF LIQUID FUEL IN A SWIRL-STABILIZED FLAME

Y. HARDALUPAS, A. M. K. P. TAYLOR and J. H. WHITELAW†

Imperial College of Science, Technology and Medicine, Mechanical Engineering Department, London SW7 2BX, England

(Received 24 February 1994)

Abstract—Mass flux, mass fraction and concentration of kerosene droplets have been measured by a phase-Doppler instrument in a swirl-stabilized burner during inert and reacting flow. In the reacting flow, the flame was supported by natural gas added through the fuel stalk, while the kerosene was added to and atomized by the combusting air. The bulk mean velocity of the combustion air was 30.4 m/s, corresponding to a Reynolds number of 30,000, and the swirl numbers were 0.48 and 0.29, respectively, upstream and downstream of the kerosene injection. The equivalence ratios were 0.45 and 2.11 for the natural gas and the kerosene, respectively. The results show that the minimum swirl necessary for flame stability caused fuel to centrifuge from the region of combustion, so that only 8 kW of energy could be released out of the available 37.4 kW of the kerosene fuel. An important conclusion is that an optimum swirl number will exist with every atomization and burner arrangement of a liquid-fuelled flame and will be different from that associated with the corresponding gas-fuelled flame. The measurement techniques appropriate to regions where the flow instantaneously reverses are described and the existence of large droplets, which moved towards the injector inside the recirculation zone and supplied fuel to the base of the flame, are explained in terms of a "fountain effect" based on the mean drag between the gas phase and the droplets. Sources of uncertainties of the mass flux and concentration measurements with the phase Doppler instrument are considered in detail.

Key Words: swirl-stabilized flame, inert flow, mass flux, mass fraction, concentration, size of liquid droplets, phase-Doppler velocimetry

1. INTRODUCTION

Some progress in the experimental investigation of liquid fuel spray flames has been made by the photographic measurements such as those of McCreath & Chigier (1973), the laser-Doppler measurements of Khalil & Whitelaw (1977), and the laser tomographic technique of Yule *et al.* (1982) but, laser-based instruments able to measure size and velocity of droplets simultaneously offer many advantages. The phase-Doppler technique, suggested by Durst & Zaré (1975), provides sizing information independent of the intensity of the laser beams and their attenuation due to the turbidity of the flow (Hardalupas *et al.* 1988), and this is important for accurate fuel flux measurements. The technique has been used successfully in non-reacting liquid sprays, for example by Bachalo *et al.* (1986), Dodge *et al.* (1988), Reitz (1988), Saffman *et al.* (1988) and Hardalupas *et al.* (1992), to measure droplet size and velocity as well as fuel flux and concentration.

Measurements in inert and reacting flows within and downstream of burner arrangements are fewer. Mao *et al.* (1986), McDonell & Samuelsen (1989), Kawazoe *et al.* (1990) and Hardalupas *et al.* (1994) used phase-Doppler velocimetry to obtain droplet flux and concentration measurements in non-swirling flows and Edwards & Rudoff (1990), Hardalupas *et al.* (1990) and Presser *et al.* (1990) in swirling flames. However, there is no emphasis in the literature on quantities related to the liquid fuel mass flux, fraction and concentration, which are associated with the ability of the liquid fuel to react and release heat in the recirculation zone and are important for the stability and extinction of the flames. Although droplet size and velocity correlations can provide information on droplet dispersion, they cannot indicate the amount of fuel present at each location. The present work focuses on mass flux, mass fraction and concentration measurements of kerosene droplets in the burner of Hardalupas *et al.* (1990) for inert and reacting flow, with the minimum

†To whom correspondence should be addressed.

swirl number required for flame stability. The emphasis is on the effect of droplet dispersion and spatial distribution on their ability to release vapour and ignite in the near burner region and, in this way, release heat to stabilize the flame. The probability of releasing the potential liquid fuel heat load in the flame is examined. A possible reason for reduced heat release is provided by Liu *et al.* (1989) who used refractive index matching of particles and liquid to show the extent to which swirl can centrifuge particles from the core region.

An important aspect of this paper is the description of the methods used to measure liquid fuel mass flux, mass fraction and concentration and the analysis of problems associated with locations within the recirculation zone, where the flow instantaneously reverses, and the measurement techniques appropriate to this region. Possible sources of uncertainties are reviewed in detail, essential to the quantification of the uncertainties, which are not available in the literature. Existing liquid fuel flux and concentration measurements in different flow arrangements are reviewed and errors associated with these measurements are evaluated. This review allows the uncertainties associated with the current measurements to be quantified.

The paper has been prepared in four sections. Section 2 describes the flow configuration and the phase-Doppler technique and methods used to measure liquid fuel mass flux, mass fraction and concentration. The sub-section concerned with the phase-Doppler velocimeter provides a description of the instrument with detail essential to the quantification of measurement uncertainties, reviews previous flux and concentration measurements and their uncertainties and quantifies the uncertainties of the current measurements. The three remaining sections present the results, related discussion and summarize important conclusions.

2. FLOW CONFIGURATION AND MEASUREMENT TECHNIQUE

The following two sub-sections describe the flow configuration and the phase-Doppler instrument used to measure droplet characteristics. Since the emphasis is on the two-phase flow results obtained by the phase-Doppler instrument, possible sources of uncertainties are considered in detail in the third sub-section and the consequences for the present measurements in the last section.

2.1. Flow Configuration

The burner was identical to that of Hardalupas *et al.* (1990) and is shown in figure 1 with dimensions and details of the fuelling arrangement. In reacting flow, the flame was supported by natural gas added through the fuel stalk. The natural gas was exchanged by air of equal momentum flowrate in the inert flow. The kerosene was injected radially through the 0.33 mm dia holes at a bulk velocity of around 2 m/s and atomized through shear with the swirling combustion air. The swirl number of the combustion air, defined as (e.g. Wall 1987):

$$\mathrm{Sw} = \frac{2G_\theta}{G_z D} \qquad [1]$$

where $G_\theta = 2\pi\rho \int_{r=0}^{R} WrUr\, \mathrm{d}r$, $G_z = 2\pi\rho \int_{r=0}^{R} UUr\, \mathrm{d}r$, R and D are, respectively, the radius and the diameter of the quarl inlet, W is the tangential velocity, U is the axial velocity and ρ is the air density, was 0.48 upstream and 0.29 downstream of the kerosene injection with the latter number estimated from the mean velocity characteristics of the 10 μm droplets. A gas-phase recirculation zone was established at the mouth of the quarl, which stabilized the flame. In the inert flow, the length of the gas phase recirculation zone was about 30% less than that of the single phase due to the introduction of the liquid fuel. The difference is likely due to the reduction of the swirl number of the air at the entrance to the quarl where liquid fuel is introduced, which arises from the loss of axial flux of angular momentum, G_θ, from the air to the kerosene droplets. In the reacting flow, the recirculation zone was 20% longer than that of the inert flow, because the smaller density of the gases in combustion reduced turbulence production and delayed the end of the recirculation zone. The flowrate of the combustion air was 315 dm^3/min resulting in a bulk mean velocity of 30.4 m/s, corresponding to a Reynolds number of 30,000, based on the bulk velocity and the diameter of the air jet at the inlet of the quarl. The flowrates of the natural gas and the kerosene were 15 dm^3/min and 0.91×10^{-3} kg/s, the latter corresponding to a potential heat release of 37.4 kW, and the equivalence ratios were 0.45 and 2.11, respectively. It is expected from the

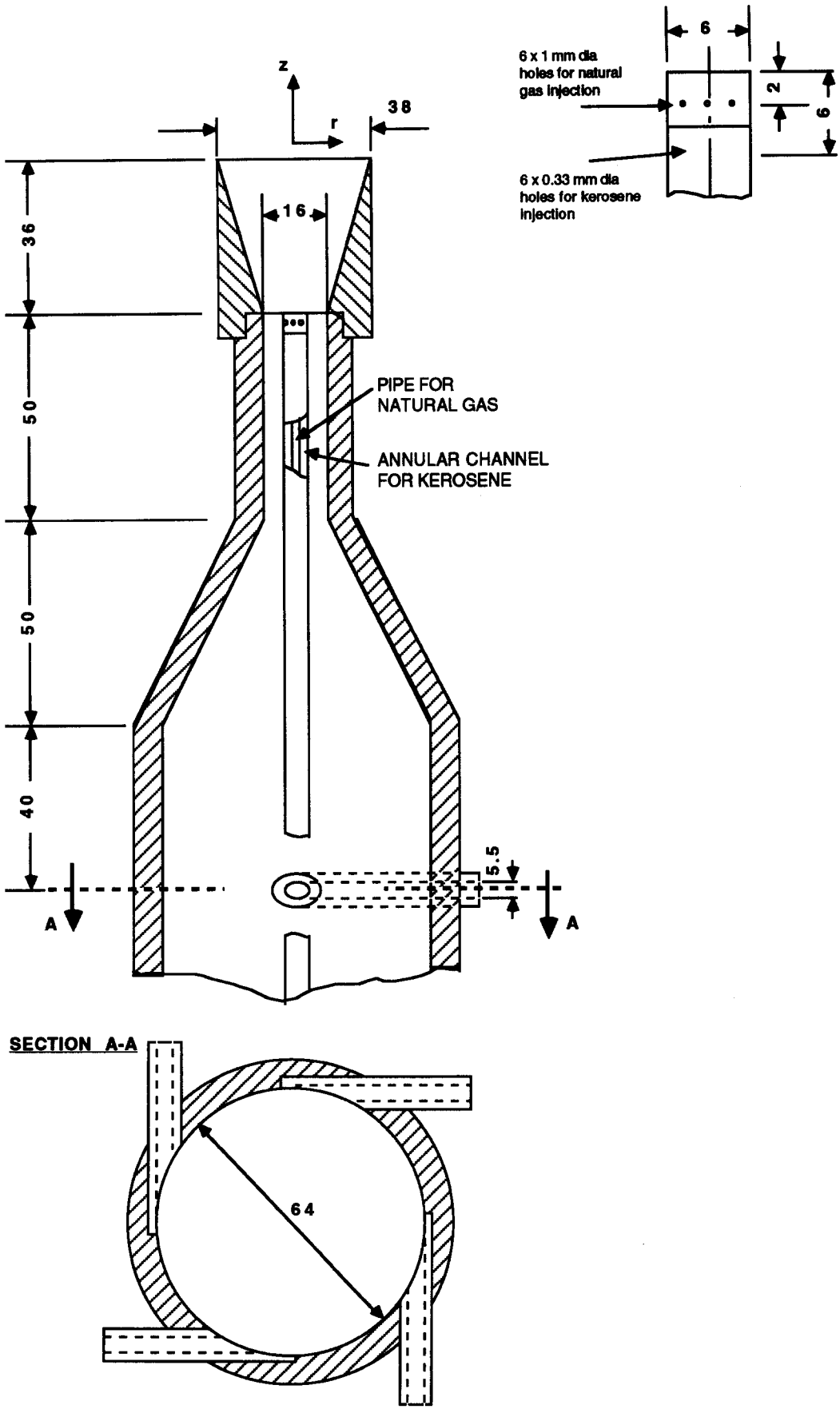

Figure 1. Geometry of the burner.

droplet velocity and size results of Hardalupas *et al.* (1990) that the potential liquid fuel heat load of 37.4 kW will not be fully released in the 8 kW gas flame and the amount of possible heat release in the recirculation zone is quantified here.

2.2. Measurement Technique

The phase-Doppler technique derives the sizing information from the spatial frequency of the interference pattern scattered by a spherical particle crossing the probe volume of a laser-Doppler velocimeter. This is measured by two photodetectors in terms of the phase shift between the resulting Doppler shift, which is linearly related to particle diameter for certain collection angles of the receiving optics. The sizing information can be obtained without calibrating the instrument before each measurement, as for amplitude-based sizing techniques (e.g. Boerner *et al.* 1986; Kliafas *et al.* 1990; Yeoman *et al.* 1982), is independent of the intensity of the laser beams and their attenuation due to the turbidity of the flow and this is important for accurate fuel flux measurements.

The phase-Doppler system used for this experiment is described by Hardalupas (1989) and was based on an Argon-ion laser, emitting light at 514.5 μm and 600 mW, transmitting optics with rotating radial diffraction grating to introduce frequency shift, and collection of the scattered light by integrated receiving optics based on three photodetectors located 30° off the axis of the transmitting optics. The beam intersection half-angle was 2.71°, the size of the probe volume was $1.71 \times 0.081 \times 0.081$ mm and the fringe spacing was 5.44 μm resulting in a frequency-to-velocity conversion factor of 0.18 MHz/(m/s). The phase to diameter conversion factor was 0.263 μm/degree which resulted in a maximum droplet diameter identified by the instrument of 95 μm. The rest of the optical and signal processing arrangements were the same as those of Hardalupas *et al.* (1990). The system provided simultaneous measurement of velocity, size, interdata arrival time and residence time of each droplet crossing the probe volume of the velocimeter and provided information of the liquid fuel mass flux, mass fraction and concentration in the inert and the reacting flow, as explained in the following paragraphs.

The phase-Doppler is a single particle counter and can measure directly the temporal size distribution. However, the effective area of the probe volume increases with particle size, because of the Gaussian irradiance distribution in the laser beams, and was calculated for each size class "i" according to Saffman (1987) and taking into account the frequency shift, as described by Hardalupas & Taylor (1989). The mass flux of a particular size class, $G'(d_i)$ (kg/m^2/s) is here defined as that crossing an area defined by having unit normal perpendicular to the plane of the fringes of the velocimeter and was calculated from the measured temporal size distribution by

$$G'(d_i) = \frac{\rho_k \pi}{6T_s} \frac{d_i^3}{A_\perp(d_i)} \sum_{j=1}^{n(d_i)} \frac{U_\perp(d_i)_j}{|U_\perp(d_i)_j|} \quad [2]$$

where ρ_k is the droplet density, T_s is the total sampling time, $A_\perp(d_i)$ is the area of the probe volume for size class d_i with unit normal perpendicular to the plane of the fringes, $U_\perp(d_i)_j$ is the jth sample of the velocity component normal to the fringes for a droplet with diameter d_i. The fraction under the summation symbol has the value $+1$ or -1 and thus provides a positive or negative sign for each measurement, depending on the sign of the velocity component, so that in the recirculation zone, where negative droplet velocities frequently predominate, the sign of $G'(d_i)$ can be negative. It should be noted carefully that the magnitude of the velocity attached to each measurement is immaterial to magnitude of the droplet flux. The net flux carried by all sizes in the distribution is

$$G = \sum_{i=1}^{k} G'(d_i) \quad [3]$$

where k is the number of bins in the size distribution. The integral of the radial profiles of net flux quantifies the liquid fuel flowrate passing through each axial station. The iso-flowrate lines, which are the equivalent of gaseous flow streamlines for the disperse phase, were drawn from the flux measurements by joining axial locations in the flow containing equal percentage of total fuel flowrate existing up to a radial distance r from the burner axis, F_r, estimated by:

$$F_r = 2\pi \int_0^r G(r) r \, dr / F_t \quad [4]$$

where r is the radial distance from the burner axis, $G(r)$ is the local net liquid fuel flux and F_t is the bulk liquid flowrate, as measured by the flowmeter. The local average mass fraction f of the liquid fuel was determined from the mass flux measurements by:

$$f = G/(G + \rho U_{air}) \quad [5]$$

where G is the local mass flux of the liquid kerosene and ρU_{air} is the local mass flux of the air. The velocity of the air in the presence of the liquid droplets, U_{air}, was approximated by that of droplets in the size range 5–10 μm and ρ is the density of the air under normal atmospheric conditions. In the reacting flow, change in gas density due to the temperature of the flow was ignored as well as the influence of the kerosene vapour and the combustion products and this leads to overestimation of the mass flux of the air by a small amount at the edge of the flame. The mass fraction of a compound in a mixture quantifies its mass transfer through an area of the flow (Spalding 1963) and can be either negative or positive and even larger than unity with the only limitation that the sum of the mass fractions of the components in the mixture should equal unity.

The number density ($\#/m^3$) of the droplets was measured independently of the flux by the method suggested by Hardalupas & Taylor (1989), which is based on the residence time of particles in the measuring volume and the number density N_i of size class "i" is given by:

$$N_i = (\Sigma\tau_i/T_s)1/V_i \quad [6]$$

where $(\Sigma\tau_i/T_s)$ is the fraction of time that the droplets of size class "i" are resident in the effective volume V_i of the probe volume of the velocimeter and T_s is the total sampling time. Any derivation of the number density of the droplets based on the division of the flux in each size class of the measured temporal size distribution by the mean velocity of each size class, as suggested by Saffman (1987) and Bachalo *et al.* (1988), exhibits discontinuity close to the free stagnation point in this flow resulting in erroneous measurements and should be avoided. The improved accuracy of the measurement of number density using the residence time technique, [6], has been recently recognized and adopted by other workers (Zhu *et al.* 1993). The concentration (kg/m^3) of the kerosene Y_k was estimated by the total number density $N(=\Sigma N_i)$ of all the measured droplets:

$$Y_k = N\pi/6D_{30}^3\rho_k \quad [7]$$

where D_{30} is the volume mean diameter calculated by the spatial size distribution and ρ_k is the density of the kerosene.

The measurements of kerosene mass flux, mass fraction and concentration were based on size distributions comprising 20,000 samples at each point and resulted in statistical uncertainty of less than 2% in the cumulative size distribution (Tate 1982), which was added to the larger measurement uncertainties discussed below and summarized in table 1.

2.3. Review of Sources of Uncertainties and Accuracy of Reported Flux Measurements

(a) Attenuation of laser beams due to turbidity of flow or optical windows

Sizing with phase-Doppler velocimetry is not affected by the turbidity of the flow (Hardalupas *et al.* 1988), because it is independent of the intensity of incident beams, in contrast to visibility

Table 1. Sources of uncertainties in the flux and concentration measurement with a phase-Doppler velocimeter

Sources of uncertainties	Influence on mass flux and concentration measurements
(a) Attenuation of laser beams due to turbidity of flow or optical windows	systematic reduction
(b) Hardware and software validation	systematic reduction
(c) Particle sizing related errors	
Multiple particles	random
Signal-to-noise ratio	random
Oscillations of response curve for small droplets	random
Gaussian intensity profile of incident laser beams	mainly systematic reduction
Droplet refractive index variation in reacting flows	systematic increase
(d) Area of probe volume	systematic increase (for estimates based on direct measurement of the length of the Doppler burst)
(e) Accuracy of the phase shift	random

and amplitude-based techniques (Kliafas *et al.* 1990). However, the mass flux and concentration measurements can be systematically reduced by an inadequate dynamic range of the photodetectors and the requirement of a minimum number of zero crossings in the Doppler signal. These possible errors can be compensated by the on-line measurement of the area of the probe volume, which is reduced as the attenuation of the laser beams increases, but not eliminated particularly in dense sprays. The magnitude of the resulting uncertainty in flux depends on the size range of the droplets and the optical arrangement used and is expected to be less than 10%.

(b) Hardware and software validation

All phase-Doppler instruments include hardware and software validation logic to eliminate signals from droplets which could lead to erroneous measurements of droplet diameter or velocity. Since the validation logic does not reject signals in a particular range of droplet diameters, the rejection rate should lead to a systematic reduction of the liquid mass flux and concentration. This uncertainty depends on the droplet number density, the signal-to-noise ratio and the logic and can be as large as 20% in most of the cases, but becomes larger for measurements in dense sprays and with low signal-to-noise ratio.

(c) Uncertainties stemming from errors in the measurement of droplet size

Droplet sizing errors can reduce or increase the flux and concentration measurements as described below.

Multiple particles. The phase-Doppler velocimeter operates properly with one droplet in the probe volume, but the probability of the presence of multiple droplets can be important in dense sprays and cause large rejection of signals with reduction of the measured flux (Edwards & Marx 1991). For certain conditions of velocity and size, however, some of those signals can still be validated (Sankar *et al.* 1993), with consequent random error in the flux measurement. This source of uncertainty has negligible effect on measurements in dilute sprays.

Signal-to-noise ratio (SNR). The accuracy of the phase measurement between two Doppler signals with a counter processor is reduced at low SNR signals (Ibrahim *et al.* 1991; Lading & Andersen 1990) resulting in random RMS errors of up to 2 degrees for SNR larger than 10 dB which doubles as the SNR is reduced to 0 dB. These uncertainties will be larger with small sizes, because of the associated small values of the phase shift.

Oscillations of response curve for small droplets. Oscillations remain on the response curve of the instrument for small droplets over a size range which varies with the optical geometry and the maximum possible droplet diameter measured by the instrument (Hardalupas & Taylor 1988; Sankar *et al.* 1991; Naqwi *et al.* 1991; Saffman *et al.* 1984). Random errors of the order of 50% may arise in the sizing of small droplets, but since they relate mainly to droplets smaller than 10 μm, which in most combustion applications carry a small amount of liquid, the effect on the flux and concentration measurements is negligible.

Gaussian intensity profile of incident laser beams. The Gaussian intensity profile of the incident beam reduces the relative contribution of refraction to the scattered light by the droplet and reflection can dominate for certain droplet trajectories with diameters of the order of the diameter of the probe volume and cause errors. Sankar & Bachalo (1991) found that about 25% of the possible droplet trajectories through the measuring volume can result in errors, which cannot be rejected by the validation logic and, for droplet diameters between 0.25 and 1 probe volume diameter, their size can be underestimated (Grehan *et al.* 1991) leading to a systematic reduction of the flux. In contrast, droplets larger than the diameter of the probe volume can be overestimated, but this error is eliminated by the sizing validation algorithm suggested by Hardalupas & Taylor (1994). The former underestimation of droplet diameter can be reduced by (i) using two receiving optical units placed symmetrically around the plane of the beams (Grehan *et al.* 1992), although alignment problems arise, (ii) appropriate optical geometry (Sankar *et al.* 1992), if this is an available option for the sizing range of the droplets measured and (iii) polarization filters which attenuate the unwanted parts of scattered light (Saffman 1986). None of these methods can eliminate the sizing errors and liquid flux and concentration may be underestimated. The resulting uncertainty in flux depends on the ratio of the droplet-to-probe volume diameter, and the

probability of droplets crossing the probe volume with specific trajectories and can be kept small if the probe volume is larger than the maximum droplet diameter in the flow.

Droplet refractive index variation in reacting flows. The increase of droplet temperature in reacting flows leads to preferential evaporation of the lighter compounds of the liquid fuel and so decreases the refractive index. Since the sizing response curve is based on the refractive index at atmospheric conditions, overestimation of diameters, flux and concentration by up to 10% can occur with a forward-scatter collection angle of 30° (Pitcher *et al.* 1991) if the refractive index is reduced from 1.4 to 1.3, which is common for hydrocarbon fuels; the overestimation increases to around 100% for backscatter collection angles (Hardalupas & Liu 1993; Schneider & Hirleman 1994).

(d) Area of probe volume calculation

Uncertainties in the area of the probe volume affect the flux and concentration measurements. Saffman (1987) calculated the area of the probe volume as a function of size from the length of the Doppler burst, determined by counting the number of zero crossings, and Hardalupas & Taylor (1989) included the effect of frequency shift which is required for measurements in regions of reverse flows. This method is limited to one-dimensional flows, and its application with a single velocity component system can lead to underestimation of the probe volume area by around 10% for droplet trajectories inclined at angles up to 60° to the direction normal to the fringes (Saffman 1987) and more than 100% for larger trajectory angles. In addition, the area of the probe volume is underestimated by up to 90% for signal-to-noise ratios (SNR) around 8 dB (Qiu & Sommerfeld 1992). According to [2], the flux measurement can be overestimated due to the area of the probe volume underestimation and the resulting error can be reduced by a two velocity component instrument, but the accepted number of measurements and the flux are reduced due to the additional requirement of time coincidence between the Doppler signals for each component and in three dimensional flows the problem appears again. An alternative method for the area of the probe volume estimation based on the detection of the amplitude of the filtered Doppler signal, has been suggested by Qiu & Sommerfeld (1992) and appears to be independent of the droplet trajectory and velocity, but more evaluation is required. The resulting overestimation of the flux depends on the probability of the inclination of droplet trajectories through the probe volume.

(e) Accuracy of the phase shift

The accuracy of the sizing measurements depends on the resolution of the electronic circuit which counts the time delay between the Doppler bursts. For a counter processor the resolution of the crystal limits the accuracy. For example, the present counter processor with resolution is ± 2 ns, defined by the 500 MHz crystal (Hardalupas 1989), resulted in $\pm 4°$ resolution of the phase measurement for a typical Doppler frequency of 6 MHz, which, after considering the sizing conversion factor of the instrument for the present optical arrangement, corresponds to $\pm 1.5\ \mu$m. This random effect is significant for droplets smaller than around 20 μm but is negligible for larger droplets. If the larger droplets carry most of the flux, the contribution to uncertainty of the flux measurement is expected to be negligible. It should be noted that FFT processors also introduce random errors because of their time resolution of the phase shift measurement, although they are more immune to errors due to signal-to-noise ratio.

Table 1 suggests that different sources of uncertainties can reduce and increase the measured flux. For example, the sizing validation can reduce the measured flux due to rejection of signals from droplets which do not meet the required criteria, but erroneous estimates of the area of the probe volume could increase the measured flux, so even after two errors, the final flux measurement could appear misleadingly correct. However, an indication of the accuracy of the flux measurement is the comparison between the estimated liquid flowrate after integration of the radial profiles of flux, assuming axisymmetric flows, with the flowrate measured by a flowmeter. Table 2 summarizes some reported measurements of flux with a phase-Doppler instrument, which include comparison between liquid flowrate supplied and estimated by integration of the measured flux profiles and indicates errors in the liquid flowrate estimates up to $\pm 20\%$ in dilute regions of the flows. In dense sprays, maximum errors between -50 and $+100\%$ can occur (e.g. Zhu *et al.* 1993; Hardalupas & Whitelaw 1993). The following conclusions can be drawn from table 2:

(i) The discrepancies are independent of the method of operation of the processor, which suggests that the accuracy of the phase shift measurement is adequate in regions of the flow where the signal to noise ratio is larger than 10 dB.

(ii) The discrepancies are mainly systematic, usually reducing the estimated flowrate, with a small random component. This justifies the assumption that systematic effects do not vary significantly in each flow and, in this way, comparisons between liquid flowrates in inert and reacting flows are possible and, for example, the evaporated fuel in reacting flows can be quantified.

(iii) The validation rate of the measurements is important and may contribute largely to the reduction of the measured flux. Correction of the flux measurements with the validation rate reduces the systematic effect and suggests uncertainties of the order of $\pm 5\%$ (e.g. Qiu & Sommerfeld 1992). This seems to be the main reason why Qiu & Sommerfeld (1992) have reported such low uncertainties in their measurements and, if the rest of the reported measurements of table 2 in dilute regions of the corresponding flow are also corrected with the validation rate, which is typically 80% of the attempted measurements, then the magnitude of the uncertainties in the *corrected* fluxes are similar to those reported by Qiu & Sommerfeld (1992).

(iv) Although it is generally accepted that the details of the method of calculation of the area of the probe volume is important for the flux measurements (e.g. McDonell & Samuelsen

Table 2. Comparison between liquid flowrate measured by flowmeters and estimated after integration of measured radial profiles of flux by phase-Doppler velocimeter

Reference	Flow configuration	Phase-Doppler system	Uncertainties of liquid flowrate measurement
Dodge *et al.* (1987)	fuel spray with 80° angle from a pressure swirl atomizer (Parker Hannifin Co., P/N 3030946)	single-velocity component with "zero crossing" counter processor	+200 to +300% at distances between 20 and 60 mm from the nozzle. Errors reduced to −20% by improving the quality of the collection lenses and increasing the width of the imaging aperture
Dodge & Schwalb (1988)	fuel spray with 80° angle from a pressure swirl atomizer (Parker Hannifin Co., P/N 3030946)	single-velocity component with "zero crossing" counter processor	−19% at a distance of 20 mm from the nozzle exit and smaller differences further downstream. *No correction with the validation ratio*
McDonell & Samuelsen (1989)	methanol-fuelled airblast atomizer with nozzle diameter $D = 6.3$ mm	two-velocity component with "zero crossing" counter processor	−36 to −8% for distances $8D$ to $16D$ from the nozzle exit *without correction with the validation ratio*
Qiu & Sommerfeld (1992)	hollow cone liquid spray from pressure atomizer	single-velocity component with fast Fourier transform processor	+5% for distances between 15 and 50 mm from the nozzle. *Correction with the ratio of the validated to the total number of measurements*
Zhu *et al.* (1993)	pressure swirl atomizer producing a hollow cone with 30° angle positioned in a swirling air stream	two-velocity component with discrete Fourier transform processor	between +100 and −40% for distances up to 50 mm from nozzle exit. Between 50 and 130 mm errors ± 10%. *No correction with the validation ratio*
Hardalupas & Whitelaw (1993)	coaxial airblast atomizers with liquid tube diameter $D = 2.3$ mm with variable liquid and air flowrates. Solid cone spray with 10° angle	single-velocity component with zero crossings counter processor including "5/8" frequency validation	−50 to −30% for distances up to $50D$. ± 10% for distances $100D$ from the nozzle exit and one case with +30% error. *No correction with the validation ratio*
Hardalupas *et al.* (1994)	isothermal flow in a bluff body liquid fuel burner with air duct diameter $D = 50.8$ mm. Spray solid cone 30° angle	single-velocity component with zero crossings counter processor including "5/8" frequency validation	−50% for distances between $0.2D$ and $1.2D$ from nozzle exit. *No correction with the validation ratio*
This work	isothermal flow in a swirl stabilized liquid fuel burner with air duct diameter $D = 16$ mm	single-velocity component with zero crossings counter processor including "5/8" frequency validation	−35% for distances between $2.5D$ and $5.2D$ from nozzle exit. *No correction with the validation ratio*

1989; Qiu & Sommerfeld 1992; Zhu *et al.* 1993), the experiments of table 2 indicate similar uncertainties from instruments using different methods for this estimate. So the conclusion of Qiu and Sommerfeld (1992) that the improvement in their flux uncertainties is due to the improved method of measuring the area of the probe volume may be misleading, and it appears that their improved accuracy was due to the presentation of their results *after* correcting them with the validation rate. Further work is required to examine the effect of the area of the probe volume on the flux measurements.

(v) In dense regions of sprays the uncertainty of flux measurements is large due to multiple particles in the probe volume, attenuation of the laser beams, low validation rate, signal-to-noise ratio and area of probe calculation. In such regions the contributions from different sources of uncertainties can become large with estimates of the liquid flowrate by integration of the flux profiles up to 100% larger than those measured in terms of the bulk flow of liquid (Zhu *et al.* 1993).

(vi) The quality of the lenses of the receiving optics is very important to the accuracy of the flux measurements. If the image of the probe volume on the aperture of the receiving optics is not well defined, droplets passing outside the part of the probe volume defined by the width of the aperture can be measured and increase misleadingly the flux (e.g. Dodge *et al.* 1987; Bachalo *et al.* 1988).

2.4. Uncertainties of the Present Measurements

Examination of each source of uncertainties in the flux and concentration measurements for the present flow quantifies the uncertainty for this experiment. The effects of the attenuation of laser beams and sizing errors due to multiple particles and the signal-to-noise ratio were negligible because the spray was dilute downstream of the exit of the quarl diffuser. Also the effects of sizing errors due to oscillations of the calibration curve for small droplets and the accuracy of the phase shift measurement were negligible since droplet diameters smaller than 15 μm carried less than 5% of the total liquid flowrate. The main sources of uncertainty and their influence are evaluated as follows:

(i) The validation rate was typically around 75% and varied $\pm 5\%$ for different parts of the flow. So the rejection rate was around 25% and systematically reduced the flux and concentration measurements.

(ii) Sizing errors due to the Gaussian intensity distribution of the laser beams could occur, since the ratio of the maximum droplet diameter to the probe volume diameter was of the order of unity ($95/81 \approx 1.2$). However, according to Grehan *et al.* (1991) mainly droplet diameters around 0.25 times the probe volume diameter can be underestimated and these droplets have diameters around 25 μm in this flow, which contribute less than 10% to the total flowrate, resulting in systematic decrease up to 5% of the mass flux and concentration measurements.

(iii) Sizing errors due to refractive index variations between 1.45 and 1.3 in the reacting flow can cause maximum errors of 10%. However, the temperature of larger droplets can be lower than that of small droplets and so the refractive index of the large droplets would be closer to that at atmospheric conditions. So the sizing error would be larger for the small rather than the large droplets and the uncertainty on the flux and concentration measurements is lower than the refractive index variation suggests, if it was the same for all droplet sizes. A systematic increase of the mass flux and concentration up to 5% is expected in the reaction zone, while the effect is negligible at the boundary of the flame, where the temperature is low.

(iv) Uncertainties in the area of the probe volume may cause a systematic increase of the flux and concentration measurements of the order of 5%, since most of the liquid droplets exist at the boundary of the recirculation where the inclination of droplet trajectories relative to the fringes of the probe volume is expected to be less than 30°.

Thus the flux and concentration measurements may be lower by around 25 and 20% in the inert and the reacting flow respectively due mainly to the rejection rate of the instrument. The integration of the measured radial profiles of liquid flux in the inert flow resulted in liquid flowrates lower than

the value measured by the flowmeter by around 35%, as shown in figure 10 after normalization by the fuel flowrate measured by the flowmeter, which supports the above error analysis, since in the inert flow a systematic reduction of 25% is expected and about 15% of the liquid fuel remained on the quarl diffuser due to wall wetting and could not be measured by the phase Doppler downstream of the quarl exit. For the reacting case, the liquid fuel flowrate was lower than that of the inert flow by around 20% due to droplet evaporation and the fuel vapour could contribute to heat release. The scatter of the results in figure 10 is caused by premature termination of data acquisition at the outer edge of the flow, where the fuel flowrate was large, rather than the sources of uncertainties discussed before and random errors are expected to be less than 10%.

3. RESULTS

The coordinate system used in the presentation of the results is shown in figure 2 together with the near field of the burner and the five measurement stations downstream of the quarl exit. The flame envelope is also shown and is an average of photographs of the flame, as will be explained later. Results are presented with axial mean velocities normalized with the area averaged air velocity in the annulus at the quarl inlet, $U_0 = 30.4$ m/s, and distances with the quarl exit diameter, $D = 38$ mm. Measurements could not be obtained beyond $r/D = +0.65$ at the last measurement station at $z/D = 1.22$, because of an obstruction to the throw of the traverse. Mass fluxes, mass fractions and concentrations have been normalized by the liquid fuel mass flux averaged over the

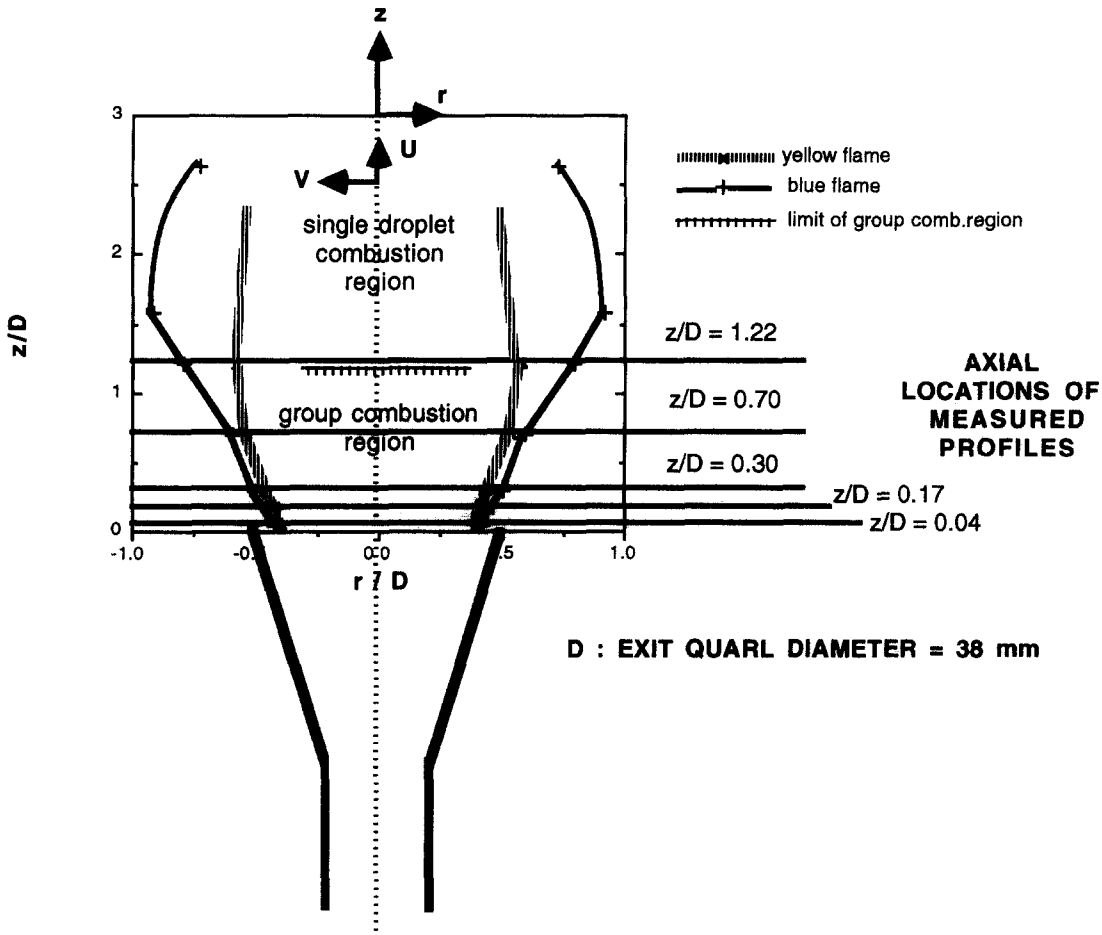

Figure 2. Sketch of the near field of the burner showing the reference system of the spatial location, the velocity and the flux, the locations where measurements were taken and the flame envelope for the reacting flow.

area at the exit of the quarl, $G_0 = 0.802\ \text{kg/m}^2\,\text{s}$, the stoichiometric mass fraction 645×10^{-4} and the kerosene density $780\ \text{kg/m}^3$, respectively. Since the mass fraction is normalized by the stoichiometric value, values larger than 1 indicate a fuel-rich region.

Results are presented for droplets in the size classes 5–10, 25–30 and 55–60 μm and after integration over all the droplet sizes. These size classes will be referred in the text as 10, 30 and 60 μm droplets and are representative of the droplet behaviour in the flow, since the 10 μm droplets follow closely the gas phase flow, the 30 μm droplets correspond to the most probable diameter in most regions and the 60 μm droplets represent the large droplets which carry most of the liquid flowrate. As will be shown, the vast majority of droplets existed at diameters less than 60 μm, although the total flux of liquid contained in smaller diameters was around half the local value at some locations. The emphasis, however, is on the region of flame stabilization, where the ability of the droplets to release heat is important and this depends on the extent to which droplets follow the flow, as characterized by the three size ranges.

The droplet response to the gas phase flow was classified by Hardalupas *et al.* (1990) according to the Stokes number, the ratio of the flow timescale to the droplet response time as follows. The ability of a droplet to respond to the gas phase flow is characterized by the response time, which is equal to the time required to accelerate to 66% of their terminal velocity:

$$\tau = \frac{\rho_L d_0^2}{18\,\mu_G} \qquad [8]$$

where ρ_L is the density of the liquid fuel, d_0 is the initial droplet diameter and μ_G is the dynamic viscosity of the gas. Values of the response time for the 10, 30 and 60 μm droplets are given in table 3, for kerosene droplets in air at atmospheric pressure and temperature. The fidelity with which a droplet is able to follow the mean and turbulent gas phase flow is quantified in terms of Stokes numbers, which are ratios of the flow timescale to the droplet response time. For example, the mean Stokes number

$$\text{St}_m = \frac{t_m}{\tau} \qquad [9]$$

with the mean flow timescale $t_m = D/U_0 = 1.3$ ms. If the gas phase is to be followed by the droplets the above parameters must be larger than unity. However, since the liquid fuel is injected radially in the annulus where it is atomized by the swirling air stream, the droplets acquire some of the angular momentum of the air and, therefore, enter the flow in the quarl diffuser with increased swirl velocity. The magnitude of the swirl velocity implies curved droplet streaklines, which can give rise to centrifuging estimated by the "centrifuge" Stokes number (Kriebel 1961; Dring & Suo 1978):

$$\text{St}_\theta = \frac{t_\theta}{\tau} \qquad [10]$$

where $t_\theta = \omega^{-1} = (W/r)^{-1}$, where ω is approximated by the angular velocity of the air estimated as the ratio of the swirling velocity component W, typically equal to $0.2U_0$ at $r = 0.25D$

Table 3. Scaling parameters for droplet evaporation and inertia characteristics

d_i (μm)	τ† (ms)	t_{ev}‡ (ms)	St_m§ (—)	St_{tr}¶ (—)	St_θ‖ (—)	t_{res}/t_{ev} pos. vel.†† (—)	t_{res}/t_{ev} neg. vel.‡‡ (—)
10	0.25	0.1	5.2	7.2	5	18	54
30	2.28	0.9	0.57	0.8	0.56	2	6
60	8.64	3.6	0.15	0.2	0.14	0.5	1.5
100	21.1	10	0.06	0.09	0.05	0.18	0.54

†From [8].
‡From [12] using $\lambda_{ev} = 10^{-6}\ \text{m}^2/\text{s}$.
§From [9] using $t_m = D/U_0 = 1.3$ ms.
¶From [11] using $t_{tr} = L_r/U_0 = 1.8$ ms.
‖From [10] using $t_\theta = (r/W)^{-1} = (0.25D/0.2U_0)^{-1} = 1.4$ ms.
††For droplets with velocity direction away from the burner $t_{res} = t_{tr} = L_r/U_0$.
‡‡For droplets which reverse their velocity direction $t_{res} = 3t_{tr}$.

(Hardalupas *et al.* 1990), to the radial distance r. Since this work focuses on the near burner aerodynamics and the ability of the droplets to evaporate and contribute to flame stability, their ability to disperse in the recirculation zone is important and related to the transit time Stokes number:

$$\mathrm{St}_{\mathrm{tr}} = \frac{t_{\mathrm{tr}}}{\tau} \qquad [11]$$

with the droplet transit time through the length L_r of the mean recirculation zone, $t_{\mathrm{tr}} = L_r/U_d = L_r/U_0 = 53\ \mathrm{mm}/30.4\ \mathrm{m/s} = 1.8\ \mathrm{ms}$ where $U_d = U_0$ is a typical droplet velocity in the spray.

Evaporation also influences the droplets in the hot environment of the recirculation zone and the lifetime of an evaporating isolated hydrocarbon droplet (Kanury 1977) is:

$$t_{\mathrm{ev}} = \frac{d_0^2}{\lambda_{\mathrm{ev}}} \qquad [12]$$

with d_0 the initial droplet diameter and λ_{ev} a parameter dependent on the surrounding gas properties, the fuel properties and the surrounding temperature. A simplification used for the purposes of this paper, justified by the high temperature of the gas in the recirculation zone, is that $\lambda_{\mathrm{ev}} = 10^{-6}\ \mathrm{m^2/s}$ for kerosene, as suggested by Kanury (1977) for a reacting droplet, and so the values of the evaporation times presented in table 3 are a minimum and will be used to evaluate fuel evaporation. Of course, evaporation times become longer in low temperature regions and in the dense droplet environment of the spray, where more complicated approaches are required (Chiu and Liu 1977; Bellan and Harstad 1987) to take into account the local oxygen and fuel vapour content and droplet number density. The droplet vapour released by the droplets in the near burner region is related to the ratio between droplet residence time, t_{res}, in the recirculation zone and the evaporation time, $t_{\mathrm{res}}/t_{\mathrm{ev}}$, which varies with the droplet diameter (Hardalupas *et al.* 1994) and if this ratio is larger than 1 the droplet evaporates completely in the recirculation zone.

The results are presented in three sections: fuel mass flux, mass fraction and concentration measurements for the inert and the reacting flow separately. In the first section the effect of the gaseous flow on the liquid fuel distribution is examined and the potential vapour release from different droplet sizes is discussed using the inert flow results and comparing with the reacting flow. The second and the third section presents the spatial distribution of the local liquid fuel mass fraction and the mass concentration, respectively.

3.1. Mass Flux

The axial and radial mass flux results are presented separately for the inert and reacting flows.

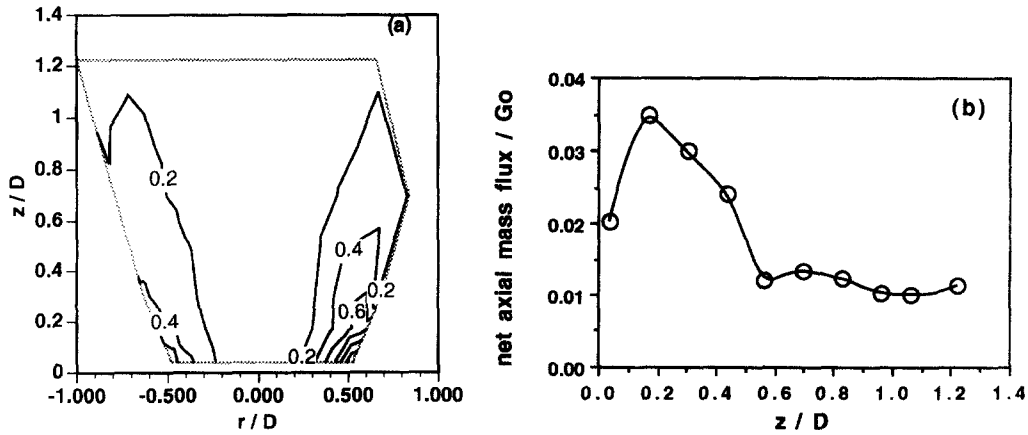

Figure 3. Net axial mass flux of the liquid fuel in the inert flow: (a) spatial distribution from the quarl diffuser exit till $z/D = 1.22$ and (b) centreline profile. Normalization by G_0, the liquid flux averaged over the area at the exit of the quarl.

(a) Inert flow

The mass flux was maximum at the edge of the jet, figure 3(a), while only a small amount of the fuel existed at the central part of the flow. Around 15% of the initial fuel flowrate reached the wall of the quarl diffuser before the exit and the amount was quantified by collecting the liquid fuel dripping downwards from the quarl over a long period. The asymmetry of the profiles was small and was traced to manufacturing tolerances in the injection holes. The centreline development is examined in figure 3(b) and the flux was large and positive close to the quarl exit and decreased sharply after $z/D \approx 0.3$, but remained always positive, indicating no recirculation zone. The results of figure 3 cannot indicate why most of the fuel exists close to the edge of the jet and if the droplets recirculate. These questions, together with the evaluation of the ability of the droplets to release vapour in the near burner region, will be answered in the rest of this section.

The air flow streamlines were calculated from the integration of the mean axial velocity measurements of the 10 μm droplets and verify the existence of a recirculation zone which extended outside the quarl to $z/D = 0.33$ and to $r/D \approx -0.3$ in the plane of the quarl exit [figure 4(a)]. The flow expanded as it came out of the quarl and air was entrained. The iso-flowrate lines of the 30 μm droplets [figure 4(b)] indicate a narrower and shorter recirculation zone than that of the air with the entrained air pushing them towards the centre, as their net radial mass flux indicates, which is towards the centre for $-0.4 < r/D < 0.4$ at $z/D = 0.3$ [figure 5(b)]. The 60 μm droplet iso-flowrate lines [figure 4(c)] close to the centreline show a small transfer of droplets towards the centre up to the end of the gas recirculation zone ($z/D \approx 0.3$), which is supported by the small net radial mass flux of 60 μm droplets towards the centreline at $z/D = 0.3$ [figure 5(c)]. However, 60 μm droplet trajectories at distances $r/D > 0.2$ only diverged and they were not affected by the entrained air flow because centrifuging due to swirl dominated. The droplets acquired swirl either during the breakup of the liquid fuel jet by the swirling air stream or during their transit time inside the quarl. The shorter length of the recirculating region of the 30 μm droplets relative to that of the gas is unexpected, since Kriebel (1961) has shown that droplets cannot follow the streamline curvature of the gas and are centrifuged away resulting in a larger radius of droplet streamline curvature. In addition to the shorter length of the 30 μm droplets recirculating region, the radius of curvature of their separation iso-flowrate line was larger than that of the gas, because the recirculation zone of the droplets was narrower. Figure 5(a) shows that the net radial mass flux of the 10 μm droplets goes towards the centreline much earlier than that of the other droplets, showing that the effect of the mean radial drag force due to the gas going towards the centreline. The velocity results of Hardalupas *et al.* (1990) indicate that the tangential velocity had a maximum far from the centreline. Thus, the small centrifugal forces on the droplets close to the centreline, allow the mean radial drag force between the gas and the droplets to disperse them towards the centreline. As the droplet size and the radial distance from the centre increases, the centrifugal force increases, and the balance of the drag and the centrifugal forces occurs closer to the centreline for larger droplets, so the behaviour of the iso-flowrate lines of the 30 and 60 μm droplets is explained. The values of the centrifuge and mean Stokes numbers for different droplet sizes (table 3) confirm the large centrifuging and the partial response of the larger droplets to the gas phase flow. Downstream of the recirculation zone, the iso-flowrate lines of the 60 μm droplets diverged from the centreline, due to increased centrifugal effect by the swirl which was acquired from the gas during the droplet transit time through the length of the recirculation zone, as indicated by the transit Stokes number of table 3, and reduced mean radial drag force acting on the droplets downstream of the recirculation zone. The iso-flowrate lines, based on the radial variation of the integral of the liquid fuel flowrate carried by all droplets [figure 4(d)], do not indicate any recirculation. It should be emphasized that zero mass flux of droplets does not imply zero velocity so that the iso-flowrate lines of the droplets do not necessarily indicate the mean trajectory of the droplet motion and mean velocity vector may not be tangential to the iso-flowrate lines.

So most of the fuel existed at the edge of the flow due to centrifuging by the swirl acquired during the breakup process of the liquid fuel jets or the transit time through the quarl and their inability to respond to the gas phase flow and be entrained towards the axis as smaller droplets do. It should be noted that the radial fuel injection arrangement of this burner injected the droplets away from the centreline in a region where the gas tangential velocity was maximum, which increased droplet

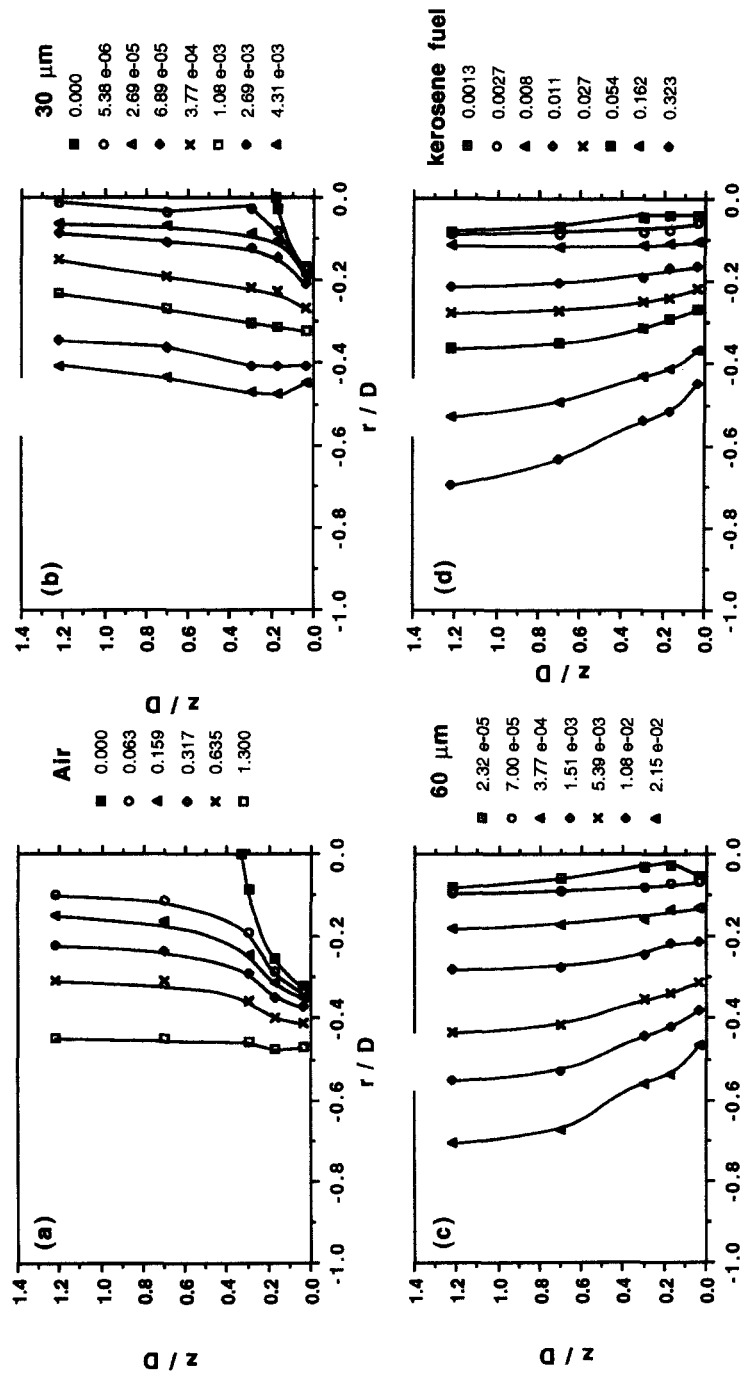

Figure 4. In the inert flow, (a) streamlines of the air flow at the presence of the liquid droplets, (b) and (c) iso-flowrate lines of the 30 and 60 μm droplets and (d) iso-flowrate lines of the total liquid fuel integrated over all the size classes. The flowrate values were normalized by the initial air flowrate 315 l/min for the air and by the bulk liquid fuel flowrate 0.070 dm^3/min for the droplets.

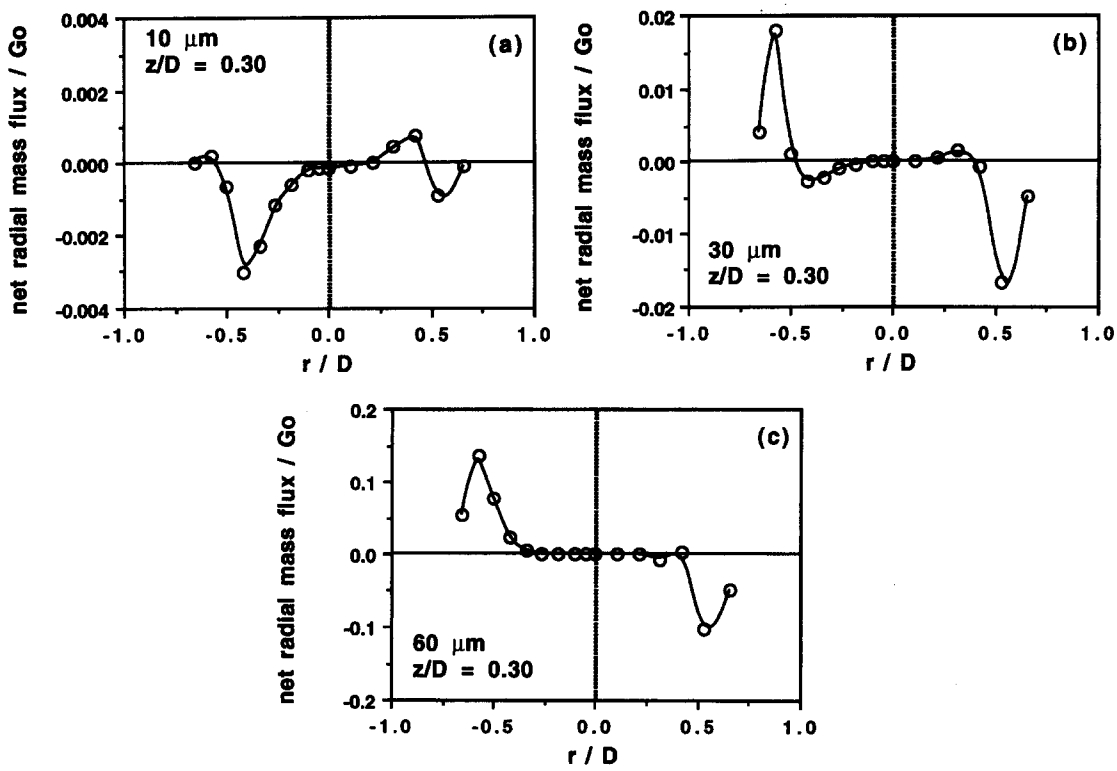

Figure 5. Radial profiles of net radial mass flux of 10, 30 and 60 μm size classes at $z/D = 0.30$ in the inert flow. Normalization by G_0.

centrifuging, but this choice resulted in symmetrical flames which did not occur for axial injection (Milosavljevic *et al.* 1990). The centrifugal effect caused larger droplets to reach the wall of the quarl diffuser.

Two remaining questions have to be answered, which are related with the ability of the droplets to reverse their velocity and the vapour that they can release in the near burner region. Since the hot region of the flame is the recirculation zone, the droplets which can contribute to the vapour release and the combustion are those existing close to the central part of the flow, $-0.4 < r/D < 0.4$. The centreline mean axial velocity for 10, 30 and 60 μm droplets [figure 6(a)], confirmed the existence of a recirculation zone which extended to $z/D \approx 0.3$ for the 10 μm droplets and thus for the gas phase. However, the recirculation zone was not evident in the net axial mass flux profiles of figure 3(a). Figure 6(b) shows that the net axial flux of the 10 and 30 μm was negative close to the burner exit and increased downstream, as the axial velocities of figure 6(a), indicating a stagnation point at $z/D \approx 0.3$ for the 10 μm droplets and at $z/D \approx 0.17$ for the 30 μm droplets. However, the 60 μm droplets had a large positive net axial flux at the exit of the quarl diffuser, which increased up to around the end of the gas phase recirculating zone ($z/D \approx 0.3$) due to the entrainment of 60 μm droplets towards the centreline and then sharply decreased downstream of the recirculation zone due to the centrifugal effect. This is in contrast to the axial velocities of the 60 μm droplets, which increased monotonically along the centreline to $z/D = 1.22$. This suggests that the 60 μm droplets with smaller axial velocity than the mean were more easily affected by the gas motion, because their transit time through the recirculation zone and the transit Stokes number increased and so did the chances to reverse their direction of movement or centrifuge from the centreline. The 60 μm droplets with axial velocity higher than the mean remained on the centreline for a longer distance and resulted in an increase of the mean axial velocity of the 60 μm droplets with the axial distance from the burner exit, although their net axial flux decreased.

The positive and negative components of the fuel mass flux carried by 10 or 30 μm droplets were of the same order of magnitude (figure 7), while the 60 μm droplets had smaller negative flux. This varies with the radial distance from the centreline (figure 8), and there was no negative flux of the

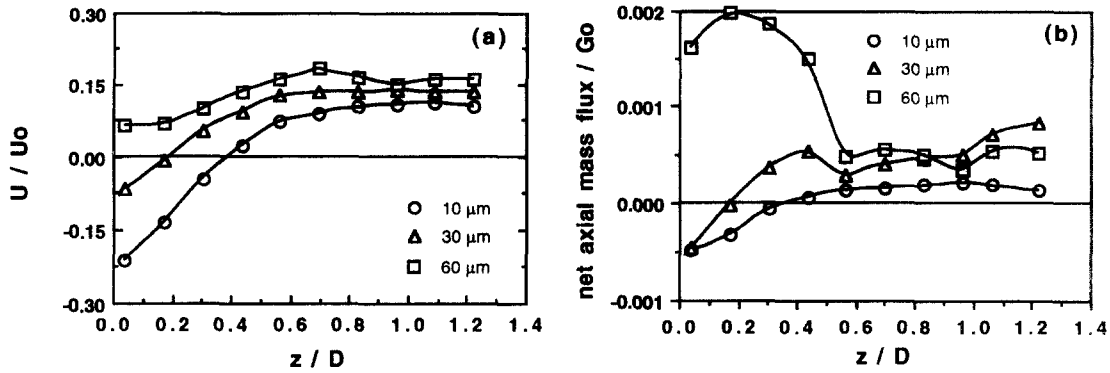

Figure 6. (a) Mean axial velocity of size classes of 10, 30 and 60 μm droplets along the centreline and (b) net axial mass flux of size classes 10, 30 and 60 μm along the centreline in the inert flow. Normalization of velocity is by U_0, the area averaged velocity at the exit of the quarl and the flux by G_0.

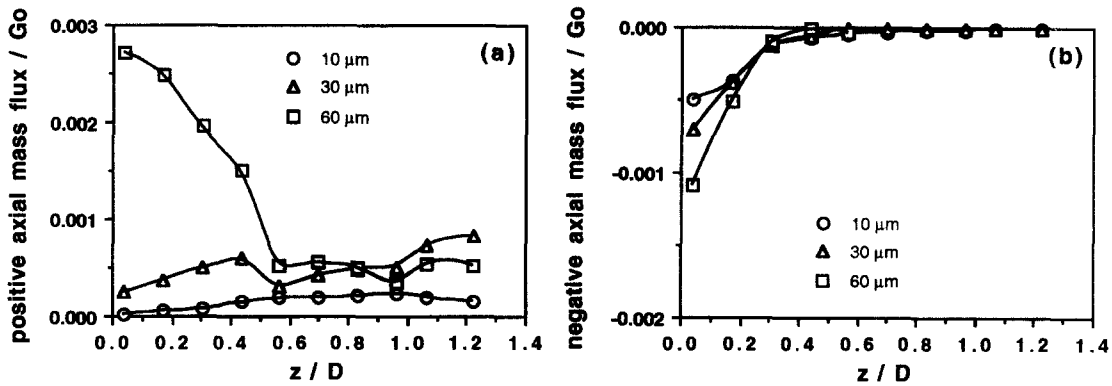

Figure 7. Centreline mass flux of 10, 30 and 60 μm size classes conditionally sampled according to the axial velocity direction of the inert flow: (a) positive, (b) negative. Normalization by G_0.

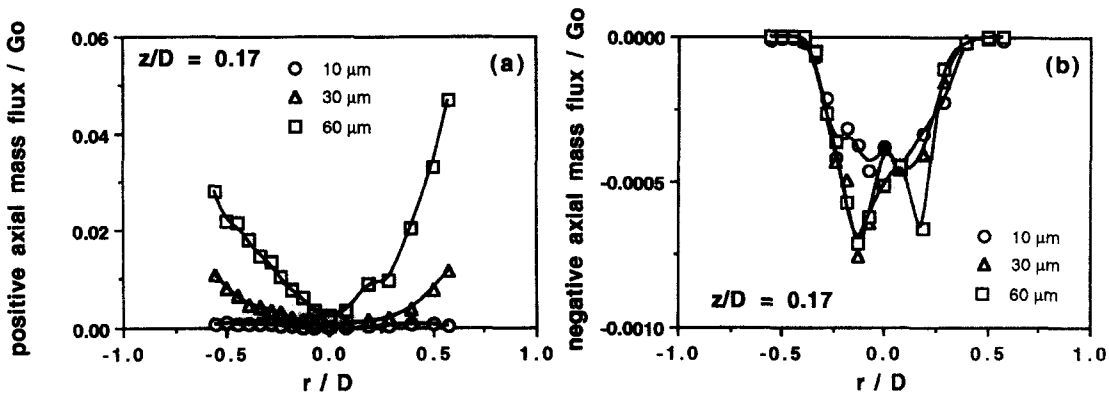

Figure 8. Radial profile of mass flux of 10, 30 and 60 μm size classes at $z/D = 0.17$ conditionally sampled according to the axial velocity direction of the inert flow: (a) positive, (b) negative. Normalization by G_0.

60 μm droplets close to the gas phase separation streamline, while 10 and 30 μm droplets still contributed to the fuel negative flux. It should be noted that the negative flux of the 60 μm was comparable and sometimes larger than that of the smaller diameters, even though their mean axial velocity was positive everywhere. So the negative flux of the larger droplets at distances between $-0/4 < r/D < 0.4$ can contribute to vapour release more than estimates on the basis of their mean velocity indicate.

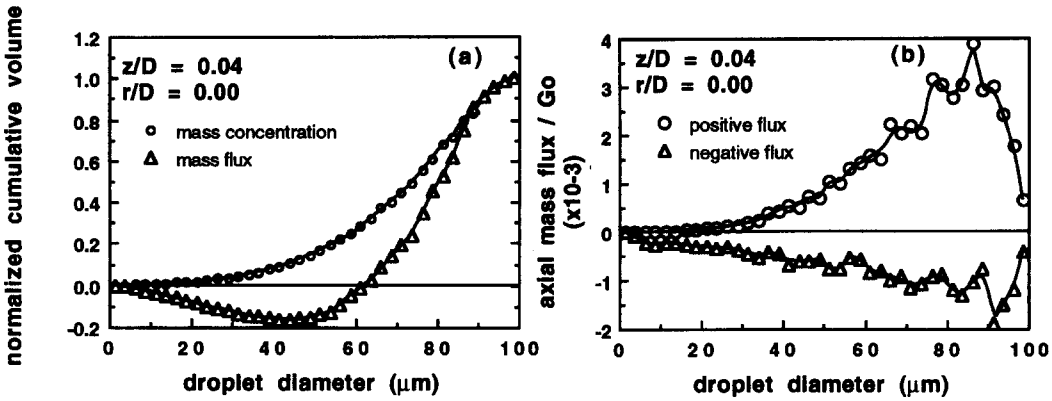

Figure 9. (a) Cumulative fuel mass flux as a function of droplet size according to the temporal and spatial size distribution and (b) contribution of the size classes to the positive and negative mass fluxes; units are in kg/m^2 s. Measurements in inert flow at $z/D = 0.04$ and $r/D = 0$.

Figure 9(a) shows the cumulative flux as a function of the size class based on the temporal and spatial size distributions, on the centreline at $z/D = 0.04$. It is evident that most of the fuel was carried by the large droplets, but it is not clear which distribution should be used to characterize the flow. Tate (1982) suggested that the spatial distribution is appropriate for combustion applications, because the fuel concentration is important for the air-to-fuel ratio. However, this does not mean that the liquid fuel available at one point is able to be burned even if there is enough air available. This might be true for droplets with a small evaporation time, but the evaporation time increases with droplet size and the residence time in the recirculation zone may become small relative to the evaporation time. Droplets which reverse their direction contribute to the negative flux and are likely to have a longer residence time in the recirculation zone and a greater chance of evaporating and burning. So it seems that the spatial size distribution is appropriate for combustion applications, where the evaporation time of the droplets is smaller than their residence time. In cases where the amount of vapour released in the recirculation zone depends on the ratio of the evaporation and the residence time, the temporal size distribution is more important, particularly for larger droplets. The temporal mass flux distribution for the negative and the positive direction as a function of size is shown in figure 9(b) and indicates that the negative flux contribution of the large droplets was larger than that of the smaller droplets and the former is likely to evaporate and burn in the reacting case, as will those droplets contributing to the positive flux, which have residence times in the recirculation zone longer than their evaporation time. The residence time of these droplets can be approximated to be three times the transit time of the droplets through the recirculation zone, assuming that droplets with reverse velocity moved towards the injector and subsequently changed direction again and left the recirculation zone. The ratio t_{res}/t_{ev} for different sizes in table 3 confirms that, for example, 60 μm droplets with negative velocity evaporated completely during their residence time in the recirculation zone, while 60 μm droplets with positive velocity did not. Since the recirculation zone extends between $-0.4 < r/D < 0.4$, figure 8(d) indicates that the liquid fuel present in this region was around 20%, from which at least 80% could evaporate. So the inert flow results suggest that about 20% of the liquid fuel can contribute to combustion, which agrees with the comparison between the liquid flowrate present in the inert and the reacting flows (figure 10), which suggests that 20% of the injected fuel became vapour and probably burned in the reacting flow.

(b) Reacting flow

The measurements of liquid mass flux in the reacting flow extended only to $r/D \approx 0.25$ (figure 11), since no droplets existed in the central region. Integration of the profiles shows that about 20% of the kerosene evaporated in the reacting flow, corresponding to a potential heat release of about 8 kW in the recirculation zone. The gradient of the net axial mass flux distributions with the distance from the centre (figure 11) was larger than that of the inert flow [figure 3(a)] showing larger

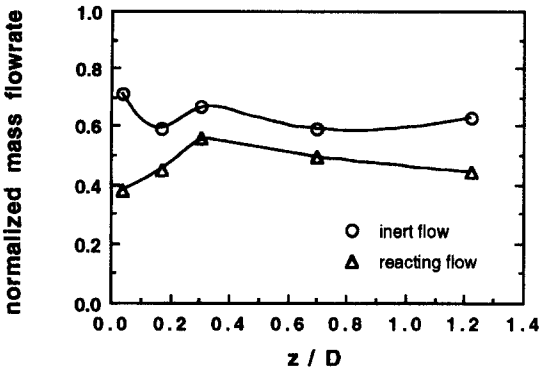

Figure 10. Liquid fuel flowrate for the inert and the reacting flow estimated after integration of the radial profiles of liquid flux at five axial stations downstream of the quarl diffuser. Normalized by the fuel flowrate measured by the flowmeter.

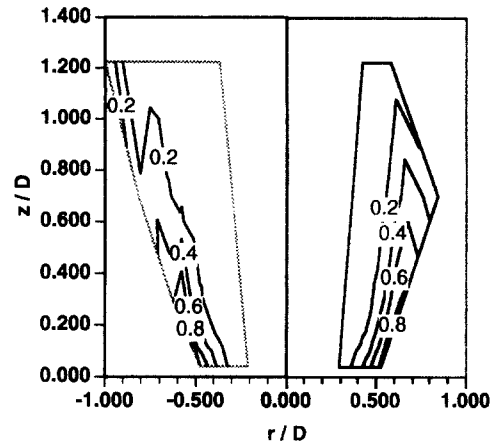

Figure 11. Spatial distribution of net axial mass flux of the liquid fuel in the reacting flow from the exit of the quarl till $z/D = 1.22$. Normalization by G_0.

evaporation close to the flame and small change at the edge of the jet where the mass flux was approximately the same as for the inert flow. The centrifuging action of the swirling air caused much of the fuel flowrate to be outside the flame envelope.

Figure 2 indicates the yellow and the blue flame envelopes, measured from photographs of the flame, with the first defining the central region of the flame where droplet combustion occurred and the latter corresponding to a flame of gas and kerosene vapour where droplet combustion did not occur. The blue flame extended to $z/D = 2.60$, where its width was $r/D = \pm 0.72$ and the yellow flame to $z/D = 1.00$, beyond which burning of single droplets was observed. The negative axial mass flux was negligibly small for all the size classes and this supports the earlier argument that

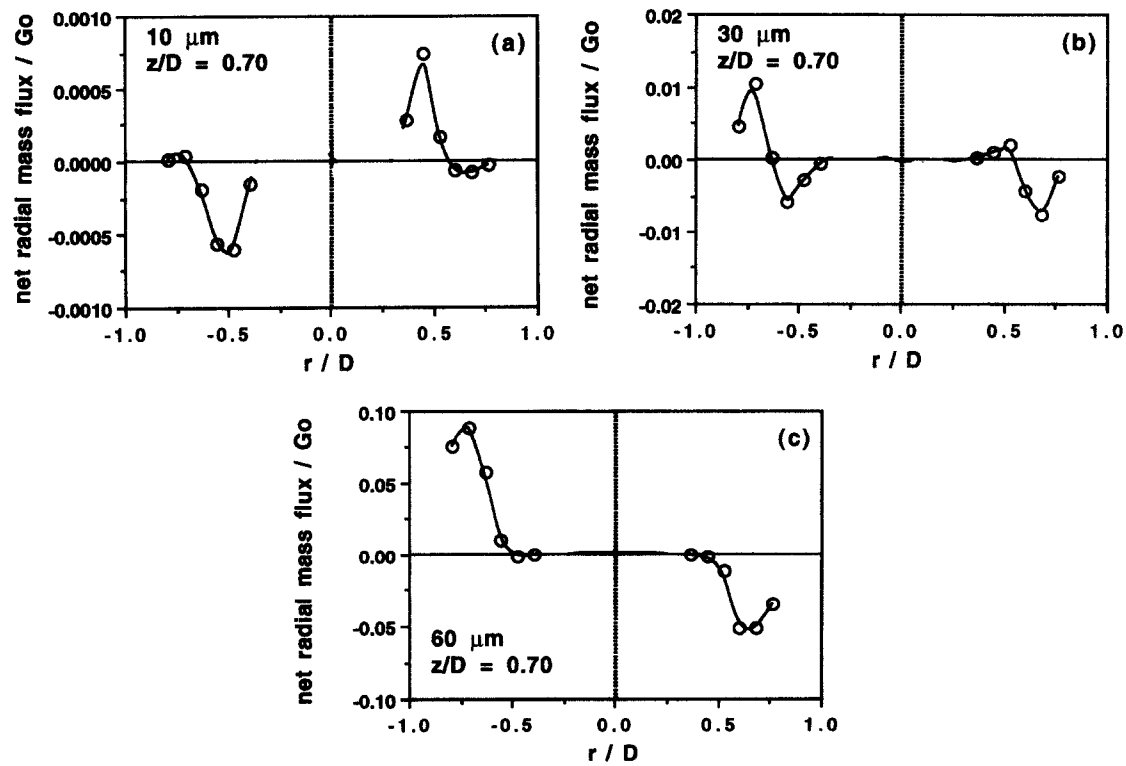

Figure 12. Radial profile of net radial mass flux of 10, 30 and 60 μm size classes at $z/D = 0.70$ in the reacting flow. Normalization by G_0.

the droplets which reversed direction had a greater chance of evaporating completely and possibly being burned in the near burner region as their residence time increased.

The net radial mass flux was also measured and is presented in figure 12 at $z/D = 0.70$ from the exit of the quarl. It is obvious that the net radial mass flux of the droplets towards the centreline in the reacting case started at larger radial distance from the centre than in the inert flow, suggesting more fuel entrained in the recirculation zone. This was probably due to preferential burning or evaporation of droplets moving from inside the recirculation zone towards the edge of the spray and crossing the flame envelope where the temperature was higher, rather than from outside the recirculation zone and towards the centreline. This resulted in detection of more droplets moving towards the centreline and explains the large net radial mass flux of liquid fuel towards the centreline. The iso-flowrate lines are not presented for the reacting flow, because the flowrate of the liquid fuel is not conserved.

3.2. Mass Fraction

The spatial distributions of the mean mass fraction of the liquid kerosene carried by all the droplet sizes and, separately, by the 10, 30 and 60 μm droplets downstream of the exit of the quarl of the burner are presented on the left and the right side of figure 13 for the reacting and the inert flow, respectively. The flow region corresponding to positive r/D is presented for both cases.

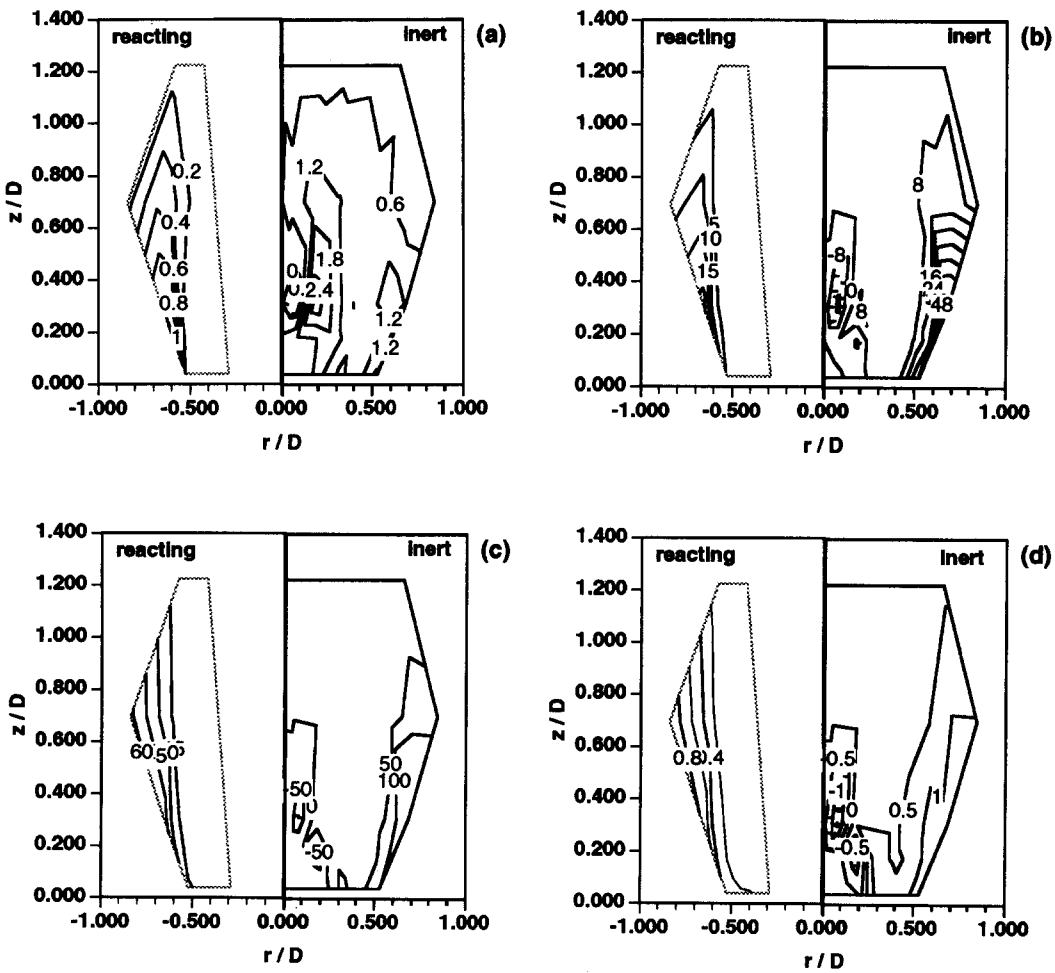

Figure 13. Spatial distributions of the local average mass fraction of the liquid fuel from the exit of the quarl till $z/D = 1.22$; the left-hand side corresponds to the reacting flow and the right-hand side to the inert flow. (a) 10 μm; (b) 30 μm; (c) 60 μm; (d) for all the droplet sizes. Normalization by the stoichiometric value of the mass fraction 645×10^{-4}. The values of graphs (a), (b) and (c) are multiplied by 10^3.

(a) Inert flow

Fuel evaporation was negligible in the inert flow, so the results indicate the local fuel-to-air ratio, which could suggest the potential ability of fuel to release vapour and react in the flame. It is not surprising that the liquid fuel mass fraction was small and negative in the recirculation zone (Spalding 1963), where only a small amount of liquid fuel entered. Close to the air separation streamline, the mass fraction was positive and large as the mean air flux was near zero and indicated a fuel-rich region of the flow [figure 13(d)] suggesting a region where the reaction could be sustained. Despite the low swirl number, diameters above about 30 μm, which represented a large proportion of the fuel volume flowrate, were centrifuged by the swirling air, so the mass fraction was large and positive at the edge of the flow where another fuel-rich region existed. Downstream of the recirculation zone, the liquid fuel mass fraction was always positive with a minimum at the centre, indicating a fuel-lean mixture as the mass flux of the air increased due to entrainment. The variation of the mass fraction of the 60 μm droplets followed that of the total liquid fuel, while that of the 30 and 10 μm droplets was small and positive inside the recirculation zone, since the net axial mass flux of the droplets there had the same sign as the air. At the edge of the jet, the mass fraction of the 30 and 10 μm droplets was reduced because they did not centrifuge and their mass flux was small.

(b) Reacting flow

The mass fraction was always positive and very small close to the centre, since most of the liquid fuel had evaporated. The values of the mass fraction at the edge of the jet were large due to the centrifuging of the fuel and similar to those of the inert flow showing that the liquid fuel, which was outside the flame envelope, was only slightly affected by the high temperature of the flame. However, the amount of liquid fuel was reduced due to droplet evaporation, since the edge of the flow was not a fuel-rich region as in the inert flow. The mass fractions of the 10 and 30 μm droplets were smaller than those of the inert flow even at the edge of the jet, indicating that most of the droplets evaporated, while the mass fraction of the 60 μm droplets, with their lower evaporation rates, was less affected.

3.3. Fuel Concentration

Number density indicates whether the droplets are burned as individual droplets or as a cloud and according to Chiu & Liu (1977), if the group combustion number, Gr:

$$\mathrm{Gr} = 3\{1 + 0.276\sqrt{\mathrm{Re}}\sqrt{\mathrm{Sc}}\}\mathrm{Le}\ N(d/2R_c) \qquad [13]$$

is much larger than 0.15, the cloud burning dominates. Here Re, Sc and Le are the Reynolds, Schmidt and Lewis numbers, N is the total number of droplets in a cloud of radius R_c and d is the droplet diameter. Assuming that Re and Le numbers are 0 and 1, respectively, then for a cloud radius of 20 mm, a typical droplet density of 0.06×10^{10} (m^{-3}) and a typical droplet diameter of 30 μm, [13] suggests cloud burning. The photographs also indicated cloud combustion in the region of measurement but that, further downstream, single droplet combustion took over. Here the results are presented in the form of mass concentration instead of droplet number density, because this quantity gives a better indication of the liquid fuel present in the flow. It should be noted that mass concentration is not a useful quantity for models based on Lagrangian tracking of particles (e.g. Gosman & Ioannides 1983), where mass flux is the appropriate quantity but it is important for Eulerian models based on second-order correlations (e.g. Shih & Lumley 1986). The spatial distributions of mass concentration of the liquid fuel for the reacting and the inert case downstream of the exit of the quarl diffuser are presented in figure 14 at the left- and right-hand side of the graphs, respectively, and are discussed separately below.

(a) Inert flow

The mass concentration was small in the recirculation zone and increased towards the edge of the jet and the centrifugal effect was again evident, since the liquid fuel mass concentration was large at the edge of the spray. Downstream of the recirculation zone, the smaller droplets were entrained towards the centreline, and the maximum concentration of 10 and 30 μm droplets was closer to the centreline while that of the 60 μm was close to the edge of the jet. So the 10 and 30 μm

droplets may be expected to burn completely, since they existed closer to the recirculation zone where the temperature in the reacting flow was high. The mass concentration of liquid fuel along the centreline decreased very rapidly close to the end of the gas recirculation zone, where the centrifugal effect was important. The concentration of 10 μm and 30 μm droplets remained near constant along the centreline and, thus, the decrease of liquid concentration was caused by the centrifuging of the large droplets due to swirl, which is confirmed by the decrease of the concentration of 60 μm droplets along the centreline.

(b) Reacting flow

The results confirm that the concentration of the liquid fuel was reduced everywhere due to droplet evaporation. Outside the central region, where no droplets existed, i.e. $r/D > \pm 0.30$, the concentration of the 10 μm droplets reduced by at least an order of magnitude, while that of the 30 μm droplets reduced by a factor of 1.5. The concentration of the 60 μm droplets reduced slightly in the region outside the flame envelope due to evaporation. The release of vapour at the edge of the flow caused a blue flame that surrounded the central yellow flame.

It should be noted that the similarity between mass fraction and concentration distributions in the reacting flow (left-hand sides of figures 13 and 14) was caused by the existence of droplets with mainly positive velocity in the flame, which resulted in non-zero values of droplet mean axial

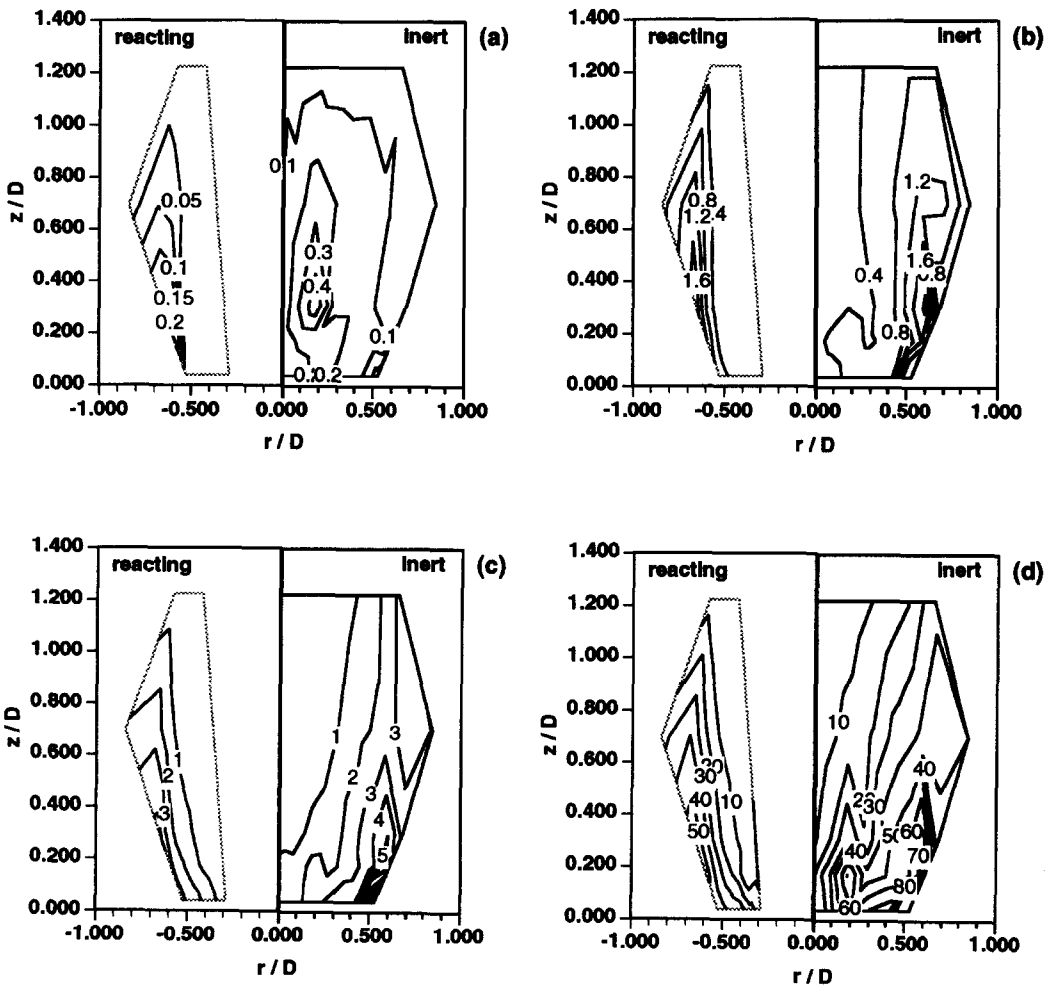

Figure 14. Spatial distributions of the local average concentration of the liquid fuel from the exit of the quarl till $z/D = 1.22$; the left-hand side corresponds to the reacting flow and the right-hand side to the inert flow. (a) 10 μm; (b) 30 μm; (c) 60 μm; (d) for all the droplet sizes. Normalization by the liquid kerosene density 780 kg/m^3. The values are multiplied by 10^6.

velocity. This justifies the assumption that the term $\overline{c'u'}$ is negligibly small in the following correlation between the time average fuel flux and concentration:

$$\overline{G(t)} = \overline{CU(t)} = \overline{C(t)}\,\overline{U(t)} + \overline{c'u'} \quad [14]$$

where the overbar denotes the time average of $G(t)$, $C(t)$ and $U(t)$, which correspond to the instantaneous mass flux, mass concentration and droplet axial velocity, respectively. Thus, [14] can be simplified:

$$\overline{G(t)} \approx \overline{C(t)}\,\overline{U(t)} \quad [15]$$

which indicates a linear relationship between liquid mass flux and mass concentration. In the inert flow, a large fraction of droplets had negative velocities, which resulted in a droplet $\overline{U(t)}$ of around zero in certain regions of the flow and $\overline{c'u'}$ plays a dominant role in [14], which cannot be simplified to [15] anymore (Hardalupas & Taylor 1989). So the relationship between mass flux and mass concentration is more complicated and the measured distributions are not similar.

4. DISCUSSION

It is evident from the results that most of the fuel flowrate was at the edge of the jet and a large fraction of the injected fuel remained unburned at $z/D = 1.22$. This stemmed from the method of atomization and the swirling component of the flow. The atomization method produced a large number of large droplets, which carried most of the fuel flowrate (figure 9) and were injected radially in order to establish a symmetrical flame (Milosavljevic *et al.* 1990). Thus, the large droplets far from the centreline acquired the swirling component of the combustion air during fuel jet breakup and their transition through the quarl diffuser and centrifuged to the edge of the jet where they remained unburned. However, the swirl number of the burner was the minimum required to stabilize the flame and the centrifuging effect could not be avoided by changing the operating conditions. It is evident that the present method of atomization is less than perfect and that, with any atomization arrangement, an optimum swirl number will exist for wide flame stability and flammability limits and high combustion efficiency and will be different from that associated with a corresponding gas-fuelled flame.

Despite the centrifugal effect, a small number of large droplets ($>30\ \mu$m) remained close to the centreline, did not have negative mean axial velocity, but contributed greatly to the negative fuel axial mass flux. Since these droplets are mainly responsible for the vapour release in the near burner region, they are important for the stability of the flame and an explanation for those negative fluxes is suggested below, since the observation is important for calculation models.

The large droplets did not recirculate because their mass did not allow them to follow the streamline curvature of the air and the iso-flowrate lines of the 60 μm droplets (figure 4) show only a small net radial flux towards the centreline. However, some of the 60 μm droplets were entrained towards the centreline or arrived there due to the initial conditions of the atomization, and rose like a "fountain". Our measurements and the transit Stokes number of table 3 suggest that the faster droplets passed through the air recirculation zone with small change of velocity and the slower ones reversed direction due to the drag of the axial air velocity, which was negative for $z/D \leqslant 0.4$. This behaviour of the large droplets is also supported by the axial velocity pdfs of the air, 30 and 60 μm droplets along the centreline (figure 15). The velocity pdfs of the 30 μm droplets and the air were skewed towards the negative velocities and gradually became Gaussian and their mean velocity increased. Those of the 60 μm droplets were skewed towards the positive velocities and the number of droplets with negative velocities gradually decreased while those with positive velocities remained the same and maintain their velocity nearly unchanged.

The mean drag between the droplets and the gas can account for the motion of the large droplets, which do not respond to the gas turbulence, if their initial conditions are known. In the recirculation zone region, the mean drag force in the radial direction dispersed the large droplets towards the centreline and the mean drag effect in the axial direction resulted in the negative flux. Our observations support the calculated particle trajectories along the centreline of a coal burner using Lagrangian particle tracking models (e.g. Smart *et al.* 1988; Godoy *et al.* 1989) and suggest that these models can be simplified by removing the interaction of large particles with the gas phase

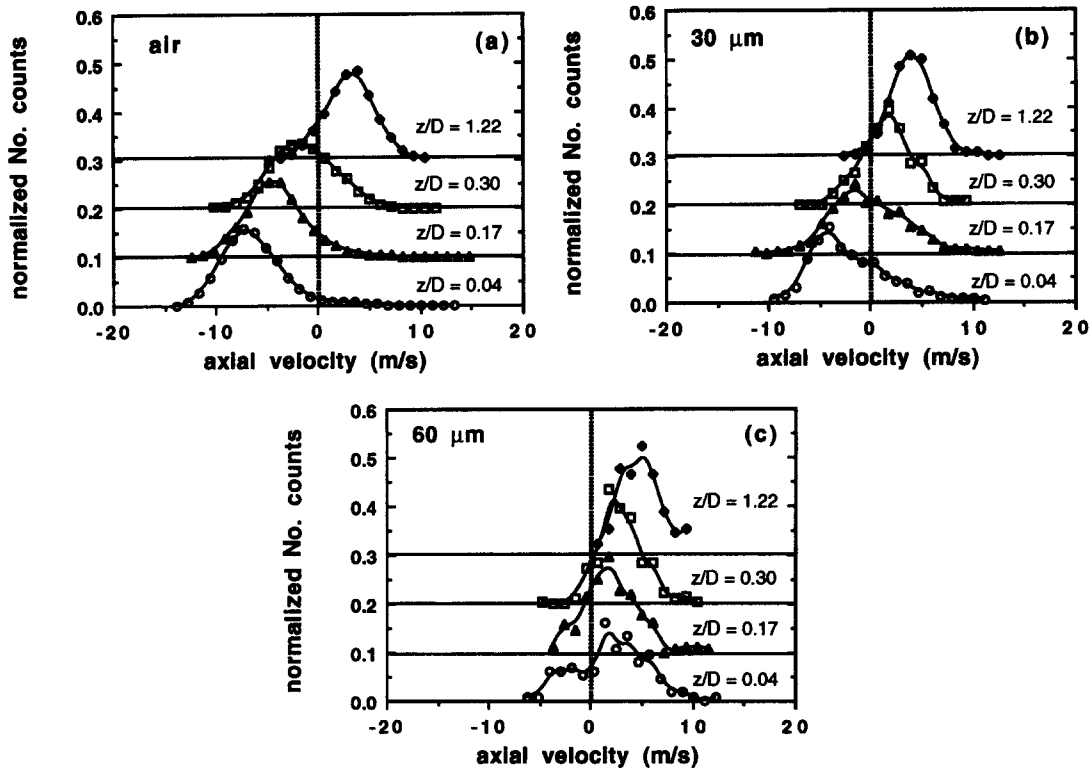

Figure 15. Velocity pdfs on the centreline at distances from the exit of the quarl $z/D = 0.04$, 0.17, 0.30 and 1.22 of (a) 10 μm, (b) 30 μm and (c) 60 μm droplets.

turbulence. In the reacting flow, the evaporation time of the large droplets must also be considered since it becomes similar to their residence time. The negative flux of the large droplets may make an important contribution to the stability of the flame as it supplies fuel to the root of the flame. It should be noted that the mass flux is a conserved quantity which has been used here to show a potential heat release of 8 kW from the liquid fuel in the recirculation zone. Thus, the temporal distribution is more appropriate than the spatial distribution for comparison with results from prediction models based on the Lagrangian tracking of droplets.

It would be nice to suggest an optimum droplet size for the geometry of this burner. A suggestion that the size of the droplets should be as low as possible, so that the droplets evaporate very quickly close to the nozzle exit, may appear attractive, but the heat absorbed by the droplets during their evaporation close to the burner reduces the flame speed and temperature (Richards and Lefebvre 1989) and may extinguish the flame. So the appropriate choice should be a droplet diameter which can partially follow the gaseous flow and avoid the centrifuging effect due to swirl and evaporate completely inside the recirculation zone but in a gradual manner. The optimum droplet diameter then appears to be around 20–30 μm.

5. CONCLUSIONS

It is evident that swirl can be necessary for flame stability but may centrifuge fuel from the region of combustion so that an optimum value may exist for each configuration, and droplet size distribution of fuel. Large droplets represent much of the mass flux and can reach the lower part of the centre of the flame to enhance stability. An optimum droplet size for this burner configuration may be around 20–30 μm, because of low centrifuging due to swirl, droplet ability to partially respond to the gas phase flow and evaporation time comparable to the droplet residence time in the recirculation zone. The following more detailed conclusions may be extracted from the preceding sections:

(1) Mass flux, mass fraction and fuel concentration have been measured by a phase-Doppler velocimeter in an unconfined swirl–burner arrangement with inert and reacting flows. The presence of kerosene and natural gas was necessary since the flame extinguished when either was removed. The results were obtained with a volumetric ratio of air-to-gas of 21 and atomized kerosene to increase the overall equivalence ratio from 0.45 to 2.53. The net mass flux of kerosene was measured by taking into account the sign of the droplet velocity and the fuel concentration from the residence time of the droplets inside the probe volume of the velocimeter. The measured spatial distributions of droplet size quantified the liquid fuel available for combustion and temporal distributions were required to identify the larger sizes, with evaporation times comparable to their residence time.
(2) The uncertainties of flux and concentration measurements with a phase-Doppler instrument were reviewed and the main source of error was the rejection rate of the validation logic of the instrument, which resulted in systematic reduction of the measurements by around 25 and 20% for the inert and the reacting flow, respectively. Random errors are of the order of 10%. However, more work is required to examine the effect of uncertainties due to the area of the probe volume calculation and the sizing errors due to the Gaussian intensity distribution of the incident laser beams.
(3) A large amount of the total liquid fuel flowrate was centrifuged to the edge of the jet due to swirl which was the minimum required for flame stability. This reduced the potential heat release of the kerosene from 37.2 to 8 kW, since only 20% of the injected liquid fuel flowrate was vaporized in the recirculation zone.
(4) Droplets larger than 50 μm contributed to the negative component of mass flux inside the recirculation zone, even though their average axial velocity was positive. The large droplets existed close to the centreline due to the initial conditions at the atomizer and their dispersion by the mean drag in the radial direction and reversed their direction due to the mean drag in the axial direction. This fountain effect explains the negative flux of large droplets which increases their residence time in the high temperature region of the recirculation zone and allows them to evaporate and contribute to the fuel vapour available for combustion in the near burner region.
(5) The average mass fraction of the liquid fuel in the reacting flow was low, as it evaporated and no droplets were found in the central region. At the edge of the jet, the mass concentration of the 10 and 30 μm droplets was greatly reduced, relative to the inert flow, while that of the 60 μm droplets was unchanged due to the preferential evaporation of the smaller droplets.
(6) The average mass fraction of the liquid fuel in the inert flow was very high around the recirculation zone and close to the edge of the spray to which a large amount of liquid fuel was centrifuged. The region downstream of the recirculation zone was fuel-lean as the air flux increased due to entrainment. The locations of the maximum fuel concentration of the 10, 30 and 60 μm droplets were increasingly displaced from the centreline, as the size increased due to the centrifugal effect.

Acknowledgements—We are grateful to the Science and Engineering Research Council and the Central Electricity Generating Board for financial support under their co-funded programme; and to the Commission of European Communities for support under contract EN3F-022-GR(TT). We would like to thank Mr V. Milosavljevic for the design of the burner and Mr J. R. Laker for the design of the electronic components of the phase-Doppler system. We are glad to acknowledge useful discussions with Dr J. Gibb of CEGB Marchwood Laboratories, and Professor G. Bergeles of the National Technical University of Athens. The second author (AMKPT) is pleased to acknowledge the Royal Society for the provision of a 1983 University Research Fellowship.

REFERENCES

BACHALO, W. D., HOUSER, M. J. & SMITH, J. N. 1986 Evolutionary behaviour of sprays produced by pressure atomisers. Paper AIAA-86-0296.

BACHALO, W. D., RUDOFF, R. C. & BRENA DE LA ROSA, A. 1988 Mass flux measurements of a high number density spray system using the phase Doppler particle analyser. Paper AIAA-88-0236.

BELLAN, J. & HARSTAD, K. 1987 Ignition of non dilute clusters of drops in convective flows. *Combust. Sci. Technol.* **53,** 75–87.

BOERNER, TH., DURST, F. & MANERO, E. 1986 LDV measurements of gas-particle confined jet flow and digital processing. In *Proceedings of 3rd International Symposium on Applications of Laser Anemometry to Fluid Mechanics*, Paper 4.5, Lisbon, Portugal.

CHIU, H. H. & LIU, T. M. 1977 Group combustion of liquid droplets. *Combust. Sci. Technol.* **17,** 127–142.

DODGE, L. G. & SCHWALB, J. A. 1988 Fuel spray evolution: comparison of experiment and CFD simulation of nonevaporating spray. Paper ASME 88-GT-27.

DODGE, L. G., RHODES, D. J. & REITZ, R. D. 1987 Drop-size measurement techniques for sprays: comparison of Malvern laser-diffraction and Aerometrics phase/Doppler. *Appl. Opt.* **26,** 2144–2154.

DRING, R. P. & SUO, M. 1978 Particle trajectories in swirling flows. *J. Energy* **2,** 232–237.

DURST, F. & ZARÉ, M. 1975 Laser Doppler measurements in two-phase flows. In *The Accuracy of Flow Measurements by Laser Doppler Methods*, pp. 403–429. Proceedings of the LDA Symposium, Copenhagen, Denmark.

EDWARDS, C. F. & MARX, K. D. 1991 Analysis of the ideal phase-Doppler system: limitations imposed by the single-particle constraint. SANDIA Report SAND91-8560.

EDWARDS, C. F. & RUDOFF, R. C. 1990 Structure of a swirl-stabilized spray flame by imaging, laser Doppler velocimetry and phase Doppler anemometry. In *23rd Symposium (International) on Combustion*, The Combustion Institute, pp. 1353–1359.

GODOY, S. G., ISMAIL, M. & LOCKWOOD, F. C. 1989 Measurements in a cylindrical pulverised coal furnace. Influence of swirl number on combustion performance. *Combust. Sci. Technol.* **67,** 59–72.

GOSMAN, A. D. & IOANNIDES, E. 1983 Aspects of computer simulation of liquid fuelled combustors. *AIAA J. Energy* **7,** 482–490.

GREHAN, G., GOUESBET, G., NAQWI, A. & DURST, F. 1991 Evaluation of phase Doppler system using generalised Lorenz–Mie theory. In *Proceedings of the International Conference on Multiphase Flows*, Tsukuba, Japan, pp. 291–294.

GREHAN, G., GOUESBET, G., NAQWI, A. & DURST, F. 1992 On elimination of the trajectory effects in phase Doppler systems. In *Proceedings of the 5th European Symposium on Particle Characterisation*, Nuremberg, Germany, pp. 309–318.

HARDALUPAS, Y. 1989 Experiments with isothermal two phase flows. Ph.D. thesis, University of London.

HARDALUPAS, Y. & LIU, C. H. 1993 Backscatter phase-Doppler anemometry for transparent non-absorbing spheres. *Exp. Fluids* **14,** 379–390.

HARDALUPAS, Y. & TAYLOR, A. M. K. P. 1988 The identification of LDA seeding particles by the phase-Doppler technique. *Exp. Fluids* **6,** 137–140.

HARDALUPAS, Y. & TAYLOR, A. M. K. P. 1989 On the measurement of particle concentration near a stagnation point. *Exp. in Fluids* **8,** 113–118.

HARDALUPAS, Y. & WHITELAW, J. H. 1993 Coaxial airblast atomizers. Final report for NASA contract NAS8-38872.

HARDALUPAS, Y., LIU, C. H. & WHITELAW, J. H. 1994 Experiments with disk stabilized kerosene-fuelled flames. *Combust. Sci. Technol.* In press.

HARDALUPAS, Y., TAYLOR, A. M. K. P. & WHITELAW, J. H. 1988 Depth of field considerations in particle sizing using the phase-Doppler technique. In *Laser Anemometry in Fluid Mechanics* (Edited by ADRIAN, R. J., ASANUMA, T., DURAO, D. F. G., DURST, F. & WHITELAW, J. H.), pp. 347–360. LADOAN—Instituto Superior Tecnico, Lisbon, Portugal.

HARDALUPAS, Y., TAYLOR, A. M. K. P. & WHITELAW, J. H. 1990 Velocity and size characteristics of liquid-fuelled flames stabilised by a swirl burner. *Proc. R. Soc. Lond.* **A428,** 129–155.

HARDALUPAS, Y., TAYLOR, A. M. K. P. & WHITELAW, J. H. 1992 Characteristics of the spray from a diesel injector. *Int. J. Multiphase Flow* **18,** 159–179.

IBRAHIM, K. M., WERTHIMER, G. D. & BACHALO, W. D. 1991 Signal processing considerations for laser Doppler and phase Doppler applications. In *Applications of Laser Techniques to Fluid Mechanics* (Edited by ADRIAN, R. J., DURAO, D. F. G., DURST, F., MAEDA, M. & WHITELAW, J. H.), pp. 291–316. Springer, Berlin.

KANURY, A. M. 1977 *Introduction to Combustion Phenomena*, 2nd edn. Gordon & Breach, New York.

KAWAZOE, H., OHSAWA, K. & FUJIKAKE, K. 1990 LDA measurement of fuel droplet sizes and velocities in a combustion field. *Combust. Flame* **82,** 151–162.

KHALIL, E. E. & WHITELAW, J. H. 1977 Aerodynamic and thermodynamic characteristics of kerosene-spray flames. In *16th Symposium (International) on Combustion*, The Combustion Institute, pp. 569–576.

KLIAFAS, Y., TAYLOR, A. M. K. P. & WHITELAW, J. H. 1990 Errors due to turbidity in particle sizing using laser Doppler anemometry. *Trans. ASME J. Fluids Engng* **112,** 142–148.

KRIEBEL, A. R. 1961 Particle trajectories in a gas centrifuge. *Trans. ASME J. Basic Engng* **83,** 333–340.

LADING, L. & ANDERSEN, K. 1990 Estimating frequency and phase for velocity and size measurements. In *Laser Anemometry: Advances and Applications* (Edited by TURNER, J. T.), pp. 161–174. BHRA (Information Services), Oxford and Springer, Berlin.

LIU, C. H., NOURI, J. M., WHITELAW, J. H. & TSE, D. G. N. 1989 Particle velocities in a swirling, confined flow. *Combust. Sci. Technol.* **86,** 131–145.

MAO, C.-P., WANG, G. & CHIGIER, N. A. 1986 An Experimental study of air-assist atomiser spray flames. In *21st Symposium (International) on Combustion*, The Combustion Institute, pp. 665–673.

MCCREATH, C. G. & CHIGIER, N. A. 1973 Liquid-spray burning in the wake of a stabiliser disc. In *14th Symposium (International) on Combustion*, The Combustion Institute, pp. 1353–1363.

MCDONELL, V. G. & SAMUELSEN, G. S. 1989 Evolution of the two-phase flow in the near field of an air-blast atomizer under reacting and non-reacting conditions. In *Applications of Laser Anemometry to Fluid Mechanics* (Edited by ADRIAN, R. J., ASANUMA, T., DURAO, D. F. G., DURST, F. & WHITELAW, J. H.), pp. 255–278. Springer, Berlin.

MILOSAVLJEVIC, V., TAYLOR, A. M. K. P. & WHITELAW, J. H. 1990 The influence of burner geometry and flow rates on the stability and symmetry of swirl stabilised non-premixed flames. *Combust. Flame* **80,** 196–208.

NAQWI, A., DURST, F. & KRAFT, G. 1991 Sizing of submicrometer particles using a phase-Doppler system. *Appl. Opt.* **30,** 4903–4913.

PITCHER, G., WIGLEY, G. & SAFFMAN, M. 1991 Sensitivity of dropsize measurements by phase Doppler anemometry to refractive index changes in combusting sprays. In *Applications of Laser Techniques to Fluid Mechanics* (Edited by ADRIAN, R. J., DURAO, D. F. G., DURST, F., MAEDA, M. & WHITELAW, J. H.), pp. 227–247. Springer, Berlin.

PRESSER, C., GUPTA, A. K., AVEDISIAN, C. T. & SEMERJIAN, H. G. 1990 Fuel property effects on the structure of spray flames. In *23rd Symposium (International) on Combustion*, The Combustion Institute, pp. 1361–1367.

QIU, H.-H. & SOMMERFELD, M. 1992 A reliable method for determining the measurement volume size and particle mass fluxes using phase-Doppler anemometry. *Exp. Fluids* **13,** 393–404.

REITZ, R. D. 1988 Effect of ambient gas conditions and turbulence on vaporising sprays. General Motors Research Laboratories, Report GMR-6158.

RICHARDS, G. A. & LEFEBVRE, A. H. 1989 Turbulent flame speeds of hydrocarbon fuel droplets in air. *Combust. Flame* **78,** 299–307.

SAFFMAN, M. 1986 The use of polarised light for optical particle sizing. In *Proceedings of the 3rd International Symposium on Applications of Laser Anemometry to Fluid Mechanics*, Lisbon, Portugal, Paper 18.2.

SAFFMAN, M. 1987 Automatic calibration of the LDA measurement volume size. *Appl. Opt.* **26,** 2592–2597.

SAFFMAN, M., BUCHHAVE, P. & TANGER, H. 1984 Simultaneous measurements of size, concentration and velocity of spherical particles by a laser Doppler method. In *Proceedings of the 2nd International Symposium on Applications of Laser Anemometry to Fluid Mechanics*, Lisbon, Portugal, Paper 8.1.

SAFFMAN, M., FRAIDL, G. K. & WIGLEY, G. 1988 Application of phase and laser Doppler anemometry to the measurement of droplet size and velocity in gasoline and Diesel fuel injection systems. In *Proceedings of the 4th International Symposium on Applications of Laser Anemometry to Fluid Mechanics*, Lisbon, Portugal, Paper 5.15.

SANKAR, S. V. & BACHALO, W. D. 1991 Response characteristics of the phase Doppler particle analyser for sizing spherical particles larger than the light wavelength. *Appl. Opt.* **30,** 1487–1496.

SANKAR, S. V., IBRAHIM, K. M. & BACHALO, W. D. 1993 Coherent scattering by multiple particles in phase Doppler interferometry. In *Proceedings of the 3rd International Congress on Optical Particle Sizing*, Yokohama, Japan, pp. 291–301.

SANKAR, S. V., INENAGA, A. S. & BACHALO, W. D. 1992 Trajectory dependent scattering in phase Doppler interferometry: minimizing and eliminating sizing errors. In *Proceedings of the 6th International Symposium on Applications of Laser Techniques to Fluid Mechanics*, Lisbon, Portugal, Paper 12.2.

SANKAR, S. V., WEBER, B. J., KAMEMOTO, D. Y. & BACHALO, W. D. 1991 Sizing fine particles with the phase Doppler interferometric technique. *Appl. Opt.* **30,** 4914–4920.

SCHNEIDER, M. & HIRLEMAN, E. D. 1994 Influence of refractive index gradients on size measurement of sperically-symmetric particles by phase-Doppler anemometry. *Appl. Opt.* In press.

SHIH, T. H. & LUMLEY, J. L. 1986 Second-order modelling of particle dispersion in a turbulent flow. *J. Fluid Mech.* **163,** 349–363.

SMART, J. P., KNILL, K. J., VISSER, B. M. & WEBER, R. 1988 Reduction of NO_x emissions in a swirled coal flame by particle injection into the internal recirculation zone. In *22nd Symposium (International) on Combustion*, The Combustion Institute, pp. 1117–1125.

SPALDING, D. B. 1963 *Convective Mass Transfer. An Introduction.* Arnold, London.

TATE, R. W. 1982 Some problems associated with the accurate representation of droplet size distributions. In *Proceedings of the 1st International Conference on Liquid Atomisation and Spray Systems (ICLASS)*, Madison, Wis., 20–24 June, pp. 341–351.

WALL, T. F. 1987 The combustion of coal as pulverized fuel through swirl burners. In *Principles of Combustion Engineering for Boilers* (Edited by LAWN, C. J.). Academic Press, London.

YEOMAN, M. L., AZZOPARDI, B. J., WHITE, H. J., BATES C. J. & ROBERTS, P. J. 1982 Optical development and application of a two colour LDA system for the simultaneous measurement of particle size and particle velocity. In *Engineering Applications of Laser Velocimetry* (Edited by COLEMAN, H. A. & PFUND, P. F.). Winter Annual Meeting ASME 1982, Phoenix, Ariz.

YULE, A. J., SENG, C. A. H., FELTON, P. G., UNGUT, A. & CHIGIER, N. A. 1982 A study of vaporising fuel sprays by laser techniques. *Combust. Flame* **44,** 71–84.

ZHU, J. Y., RUDOFF, R. C., BACHALO, E. J. & BACHALO, W. D. 1993 Number density and mass flux measurements using the phase Doppler particle analyser in reacting and non-reacting swirling flows. Paper AIAA-93-0361.